ISSN 1016-6254

Österreichische Beiträge zu Meteorologie und Geophysik

Heft 34

PHYSICAL PROCESSES, MODELLING AND MEASURING OF ICING EFFECTS IN EUROPE

Hartwig Dobesch, Dimitar Nikolov, Lasse Makkonen

Wien 2005

Österreichische Beiträge zu
Meteorologie und Geophysik

Heft 34

PHYSICAL PROCESSES, MODELLING AND MEASURING OF ICING EFFECTS IN EUROPE

Wien 2005

Zentralanstalt für Meteorologie und Geodynamik, Wien

Publ.Nr. 415

ISSN 1016-6254

IMPRESSUM

Herausgeber: Zentralanstalt für Meteorologie und Geodynamik (ZAMG), Wien

Leitende Redakteure: Sophie Debit, Fritz Neuwirth, ZAMG, Wien

für den Inhalt verantwortlich:
Hartwig Dobesch, Dimitar Nikolov, Lasse Makkonen

Druck: Grafisches Zentrum HTU GmbH
1040 Wien, Wiedener Hauptstraße 8-10
www.grafischeszentrum.at

Verlag: Zentralanstalt für Meteorologie und Geodynamik
Hohe Warte 38, A-1190 Wien
Austria (Österreich)

PHYSICAL PROCESSES, MODELLING AND MEASURING OF ICING EFFECTS IN EUROPE

CONTENTS

Summary

In this study general information about the icing conditions at the investigated test site near a wind turbine in the region of Oberstrahlbach, Austria, are given and an inventory of icing model results is presented. In addition, an overview of the physical processes involved in icing is compiled. Some estimations of the accreted ice mass based on the described models, such as for freezing rain and in-cloud icing with the measured meteorological parameters are presented. These measurements involved experimental data for the winters 2002/03 and 2003/04 at several levels on a meteorological mast together with pictures from web cams to collect information from which icing and visibility could be directly assessed. The results show that some icing models can be used with good success. However the available on-site measured meteorological data are not sufficient for a detailed modelling of the icing process, which would require input information about the droplet size distribution, and the liquid water content. These properties can only be partly derived from the investigated models and algorithms.

Keywords:

Icing, ice accretion, icing models, icing measurements, atmospheric ice.

Acknowledgement

This work is based on measurements and results from the project "*Wind Turbines in Icing Environment: Improvement of Tools for Siting, Certification and Operation (NEW ICETOOLS)*", granted by the European Union in the Field of specific program for RTD and demonstration on "Energy, Environment and Sustainable Development – Part B: Energy program" under the contract No. NNE5/2001/259.

Authors

Hartwig Dobesch, Central Institute for Meteorology and Geodynamics, Vienna;
hartwig.dobesch@zamg.ac.at

Dimitar Nikolov, National Institute of Meteorology and Hydrology; Sofia;
dimitar.nikolov@meteo.bg

Lasse Makkonen, Technical Research Centre of Finland, VTT, Espoo;
lasse.makkonen@vvt.fi

List of Parameters used

A	cross sectional area of the object (m^2)
α_1 or E	collision efficiency
α_2	sticking efficiency
α_3	accretion efficiency
β	coefficient of freezing
c_p	specific heat of air at constant pressure (J/kg°C)
c_w	specific heat of water (J/kg°C)
C_D	drag coefficient
d	diameter of droplets (μm)
d_f	diameter of snowflakes (μm)
D	diameter of the obstacle (m)
d_{id}	minor axis of the ice deposition (m)
D_{id}	major axis of the ice deposition (m)
D_i	diameter of the icicle (m)
e_0	saturation vapour pressure of air over water at T=0°C (hPa)
e_a	saturation vapour pressures over water at t_a (hPa)
h	convective heat-transfer coefficient,
h_d	thickness of the deposition (m)
I	intensity of ice accretion (kg/m^2s)
k_a	molecular thermal conductivity (W/m °C)
L_e	latent heat of evaporation (J/Kg)
L_f	latent heat of freezing (J/kg)
M	ice mass deposition, (kg/m^2)
μ_a	dynamic viscosity of the air (kg/m.s)
n	freezing factor
N	total number of droplets in $1cm^3$
θ	angle of droplet impact (degree)
P	precipitation intensity (mm/h)
q_{index}	heat fluxes in the heat balance equation (W/m^2)
r_d	droplet radius (μ)
Re	Reynolds number
R_{eq}	equivalent radial thickness (m)
R_0	radius of the cylinder (m)
R_w^*	runback mass flux (kg/m^2s)
ρ	density of ice (kg/m^3)
ρ_a	density of air (kg/m^3)
ρ_d	density of droplets (kg/m^3)
ρ_w	water density (kg/m^3)
S	surface area of the obstacle (m^2)
Stk	Stokes number
σ	Boltzmann constant ($5.67\times10^{-8}Wm^{-2}K^{-4}$)
t_a	air temperature (°C)
t_d	temperature of the droplets (°C)
t_s	temperature of the icing surface (°C)
u	velocity of the airflow (m/s)
V	wind speed (m/s)
v_d	velocity of droplets (m/s)
v_T	terminal impact velocity of the droplets (m/s)
Vis	visibility (m)
w or LWC	liquid water content of the air (kg/m^3)

1. Introduction

Icing is a meteorological phenomenon, which can affect different sectors of human activity, such as energy production and transmission, telecommunication networks, as well as land, air and marine traffic. If the icing event is severe the whole structure of social and economic life in the affected area can be heavily influenced. An example of such a case is the last extreme icing in January 1998 in North East Canada.

Icing loads have always to be taken into account in the design of technical equipment in regions where this phenomenon occurs frequently. For the estimation of icing effects the availability of accurately measured data series over sufficient time are necessary. However, such data are rare and usually have a too low spatial and temporal resolution to be used for estimating ice loads routinely. Therefore, different icing models, using data from meteorological measurement networks are used as a tool to estimate the possible ice loads.

In recent years considerable work on the theory of icing and in the modelling of the process has been made. Due to the serious impact on people that the icing of powerlines has, most of the icing models have been developed for this specific purpose. Such models have been presented by Ahti and Makkonen.(1982), Chaine et al.(1974), Gluchov (1989), McKay and Thompson(1969), Stanev and Moraliiski (1987), Jones (1996), Makkonen (1981, 1984, 1998). With the development in recent years of the wind energy sector, models for the assessment of icing on turbine blades have become as important (Makkonen et al., 2001).

1.1 Types of icing

Atmospheric icing can be classified according to the meteorological conditions and properties of the air particles by two different formation processes:

- Precipitation icing.
- In-cloud icing.

However, a classification may also be based on prevailing meteorological conditions, as given in ISO 12494 (2000). According to these conditions during icing, the physical properties and the appearance of the accreted ice will vary widely. The amount of accreted ice will depend on several factors, the most important being temperature, wind and the duration of ice accretion. Furthermore, a main precondition for a particular ice accretion are the dimensions of the object exposed and its orientation to the wind.

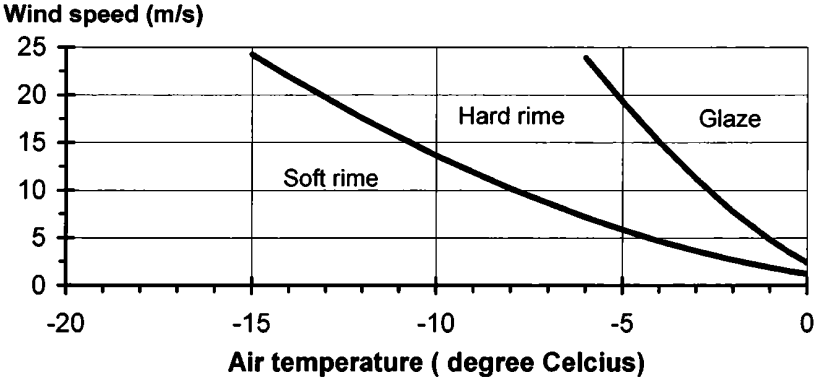

Figure 1.1: Type of accreted ice as a function of wind speed and air temperature after ISO 12494

The curves in Figure 1.1 shift to the left with increasing liquid water content and with decreasing object size.

From the general classification of icing in ISO 12494 (2000) we have:

- Glaze

This is a typical deposition by the wet growth process, having the highest density and is caused by freezing rain, freezing drizzle or wet in-cloud icing and normally creates smooth evenly distributed ice accretion. It may also give rise to the formation of icicles and can be accreted on objects anywhere when rain or drizzle occurs at temperatures below freezing point. It is formed most often at temperatures between 0 and –4°C The structure of the deposition has usually high density and is clear, transparent or opaque. This type of icing possesses a strong force of adhesion.

- Wet snow

This kind of icing occurs if the snowflakes contain liquid water. Due to the occurrence of free water in the partly melted snow crystals wet snow is able to adhere to the surface of an object. Wet snow accretion therefore occurs when the air temperature is just above the freezing point. The density of wet snow deposits depend on the fraction of melted water and wind speed varying between 300 and 500 kg/m^3.

- Rime

Rime (or in-cloud icing) is the most common type of in-cloud icing and refers to icing events caused by deposition of super cooled fog or cloud droplets. By low temperatures and small droplets the structure of deposition results in fragile ice with low density. It often forms vanes on the windward side of objects. The most severe rime icing occurs on freely exposed mountains or where mountain valleys force moist air through passes, that consequently both lifts the air and increases wind speed over the pass. The accretion rate for rime mainly varies with the dimensions of the object exposed, the air temperature and the droplet size. When the droplets are larger and the air temperature higher, the deposit is usually opaque with higher density. Thus the rime ice can be divided into two subtypes – soft and hard rime (see Table 1.1).

- Other types of ice

Hoar frost, which is due to direct phase transition from water vapour into ice (sublimation), is also common at low temperatures. It is of low density and strength, and normally does not result in significant loads on structures.

In the following table the main properties of the ice types are compiled.

Table 1.1: Typical properties of accreted atmospheric ice, after ISO 12494 (2000)

Type of ice	Density [kg/m^3]	Adhesion & Cohesion	General Appearance	
			Color	Shape
Glaze	900	strong	transparent	evenly distributed/ icicles
Wet snow	300-600	weak (forming) strong (frozen)	white	evenly distributed/ asymmetric
Hard rime	600-900	strong	opaque	asymmetric, pointing windward
Soft rime	200-600	low to medium	white	Asymmetric, pointing windward

1.2 Effects of icing

The general effects of icing are increased vertical loads on the iced structure and wind drag due to the increase in exposed area. The latter may lead to more severe wind loads than without icing. As stated in ISO 12494 (2000) the following processes have to be taken into considerations for estimating the actual ice loads on a specific object:

- Static ice loads

The sensitivity of objects to ice loads is dependent on type of structure and the varying aspects of icing. This gives a wide variety of possible influences on these objects.

- Wind action on iced structures

Wind action on iced structures can be estimated by the same principles as the action on the ice-free structure. However, both the dimensions of the structural members and their drag coefficients are subject to change. The main purpose of ISO 12494 is to specify viable values for dimensions and weight of accreted ice, shapes of accreted ice and drag coefficients of accreted ice.

- Dynamic effects

A significant factor influencing the dynamic behavior of a structure is its resonance frequency. Normally the resonance frequencies of a structure are decreased considerably if the structure is heavily iced. This is important because the lower frequencies normally are the critical ones and in addition the change in cross sectional shape due to the accreted ice may require dynamic investigations to be made. Shedding of ice from a structure may cause severe dynamic effects and stresses in the structure, depending on the type of structure and the amount and properties of the ice.

- Damage caused by falling ice

Experience shows that the shedding of ice from a structure typically occurs during increasing temperatures. Normally, accreted ice does not melt from the structure, but breaks away in fragments because of small deflections, vibrations, etc. usually results in increased risk of damage which can be reduced by shielding structures. An increased height from which the ice falls is an

important factor when evaluating risks of damage, as a greater height results in greater dynamic forces from the ice.

1.3 Ice classes

To be able to express the expected amount of accreted ice at a specific site, the term ice class (IC) is introduced (cf. ISO 12494, 2000). These can be derived on the base of meteorological parameters together with the physical properties of ice and the icing duration The icing severity can therefore be defined for a certain ice class, which defines how much ice can be expected for dimensioning purposes.

The ICs are defined by the value of the 50 year return period of the ice accretion on the reference collector. This reference collector is a 30 mm diameter cylinder of a length not less than 0,5 m, placed 10 m above terrain and slowly rotating around its own axis.

ICs can be quantified by:

- Meteorological and/or topographical data together with use of an ice accretion model, or

- Ice masses (weight) per m structural length, measured on site.

In the ISO 12494 the ICs are defined for both glaze and rime, because characteristics for these differ. ICG denotes glaze deposits and ICR rime deposits, wet snow is here treated as rime.

2. Physical processes involved in icing

Icing is the physical process of either the deposition of super cooled rain or fog droplets and their subsequent freezing on an obstacle, or the direct ice sublimation from the vapour phase.

The icing process can be divided in two main phases, which are governed by different physical mechanisms. The first one is the moving and deposition of super cooled water droplets and the second one is the transition from liquid to solid phase at freezing.

The first phase is determined by the aerodynamic properties of the droplets, the obstacle and the airflow around the obstacle. These characteristics determine what part of the droplets mass from the total water flux will be deposited on the obstacle and what part will be deviated or bounced from the obstacle.

The second phase is governed by the thermo-dynamical characteristics of the impinging droplets, the surface of the obstacle, the deposited ice and the surrounding environment. These conditions determine what part of the deposited water can be frozen.

There is interdependence between these two mechanisms. Increasing wind speed may lead to a change of the thermal conditions of the ice surface, increasing the water flux and the water-phase mixture of the air particles, important processes affecting bouncing from the obstacle (especially in cases of wet snow accretion).

Another important factor in an icing process is the water flux impinging on the obstacle, which is determined by the liquid water content of the air or the mass of water in droplets with different diameters in a unit of air volume

All these factors determine not only the rate of ice accumulation but also affect the structure and density of the deposition.

2.1 The icing rate

The icing rate is defined as the mass (M) of the ice deposit accreted on the surface of an object per unit time. If one considers an air flow perpendicular to a cylinder (see Figure 2.1), then the maximum amount of water that could deposit on the surface per unit length and unit time will be the product of the liquid water content of the air, the wind speed (V) and the diameter of the cylinder (D)

$$I = \frac{dM}{dt} = EwVD, \tag{2.1}$$

where w is taken in kg/m^3, V in m/s and D in m.

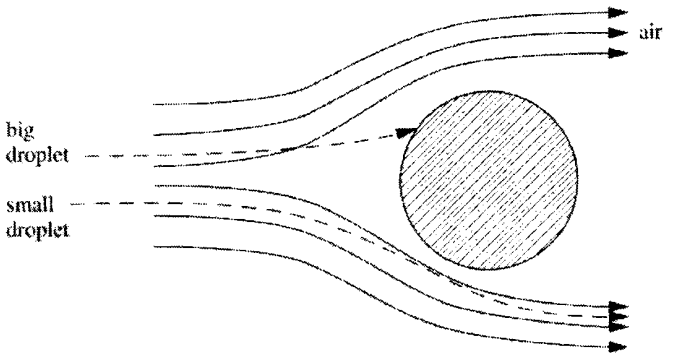

Figure 2.1: Air streamlines and droplet trajectories around a cylindrical object (after Makkonen 2000)

The correction factor E (collision efficiency) has values from 0 to 1 and represents the fact that the rate of icing dM/dt may deviate from its maximum theoretical value. The main factor determining E is the collection coefficient i.e. the part of the droplets impinging on the surface of the obstacle. E is unity if all particles in the geometrical shadow of the obstacle hit its surface. However only some of them can reach the surface and these are the bigger droplets, whilst the smaller will be deflected with the stream lines around the object (Figure 2.1). Some of the droplets reach the surface but may bounce off. In addition, reduction of the icing rate by losses of the previously deposited water is possible. This is due to losses by shedding or dripping before the deposited water can freeze. These losses are mainly coupled with the water flux density to the surface, which can be expressed as the product of the liquid water content and the air velocity. If the water flux density is too high, then the thermo-dynamical balance does not allow the freezing of all the available water. In this case, the deposited water remains on the surface until the surface tensional forces are overcome by gravitation or wind drag.

The whole process of icing from the initial deposition of super cooled water droplets to the final ice deposit can be described sufficiently well only if all the above factors are taken into account.

In order to assess these factors different approaches have been made.

Mazin (1957) introduced the coefficient of freezing β, which is expressed as

$$\beta = 1 - \frac{m_i}{m_b} \tag{2.2}$$

Here m_i is the mass flux impinging the surface and m_b the mass of water evaporated simultaneously.

List (1977) proposed the process of ice increasing to be expressed by E_{net}, which he defined as the ratio of the net icing growth rate to the total droplet mass flux.

Considering the wet growth process Makkonen (1981) described the process in terms of icing efficiency E_i as the product of the accretion E_a and the collision E efficiency as $E_i = E_a E$.

More generally, E can be expressed (Makkonen, 2000) in the form $E = \alpha_1 \alpha_2 \alpha_3$ and the icing rate as

$$I = \alpha_1 \alpha_2 \alpha_3 w V A, \tag{2.3}$$

where α_1 is the collision efficiency, α_2 the sticking efficiency and α_3 the accretion efficiency.

2.2 Motion of icing particles in the airflow around an obstacle

2.2.1 Aerodynamic characteristics

For describing an icing process it is important to know the aerodynamic characteristics of the airflow around an obstacle. In most icing models potential flow is assumed. Accordingly, Poots (1996) suggested that the motion of the icing particles does not affect the steady flow around an obstacle except near the surface. He compared the thickness of a viscous laminar boundary layer attached to a bluff surface with the icing particle size and found that this layer will be greatly disturbed by freezing raindrops.

The aerodynamic characteristic of the airflow and the icing particles, as well as the dimension of the obstacle determine, which part of the net liquid water flux density will impinge on the surface exposed to the wind i.e. the collision efficiency α_1. The probability for a droplet to reach the obstacle surface and not to be deflected around the obstacle depends on the size of the droplet and the obstacle and on the velocity of the air stream. The droplets, which possess a larger moment of inertia, will more probably reach the surface, while the small droplets will be deflected with the streamlines. The collision efficiency can be defined as the ratio of the amount of the droplets impinging the obstacle surface to the net amount of the droplets comprised in the windward cross section of the obstacle.

The first calculation of the collision efficiency for in-cloud icing were initiated by Taylor (1940), Langmuir and Blodgett (1946) and Mazin (1957) during investigations for aircraft icing. The main goal was here to determine the conditions under which the droplets strike the surface of the obstacle and the distribution of the deposited water around it. They examined the motion of droplets in a potential flow attached around a cylinder. In the equation of motion for in-cloud icing the gravitational and the buoyancy forces could be neglected, assuming Stokes drag force only. Considering the motion of particle flow perpendicular to a cylinder with radius r_0 the equation of motion has the following form

$$\frac{4}{3}\pi r_d^{\,3}\rho_d\frac{dv_d}{dt}=6\pi\mu_a(u-v_d)\left(\frac{C_D\,\mathrm{Re}_d}{24}\right) \tag{2.4}$$

with the boundary conditions $v_d \to U_i$ if $|r| \to \infty$.

Here r_d is the droplet radius (μ), ρ_d the density of droplets (kg/m^3), v_d the velocity of droplets (m/sec), u the velocity of the airflow, μ_a the dynamic viscosity of the air (kg/m s), U_i the free stream velocity and $\boldsymbol{r}$ is radius vector. This equation is usually written in dimensionless variables.

The coefficient $C_D Re_d/24$ could be assumed as indicator for the degree of deviation from the Stokes' Law in the force which moves the droplets. If Stokes' Law is in force ($Re_d << 1$) this coefficient is unity. If the Stokes' Law can not be applied, the force acting on the droplets increases. In this case $Re_d >> 1$ and then it can be expressed by the following empirical formula

$$\left(\frac{C_D\,\mathrm{Re}_d}{24}\right)=1+0.197\,\mathrm{Re}_d^{0.63}+2.6*10^{-4}\,\mathrm{Re}_d^{1.38} \tag{2.5}$$

Investigations of the droplets motion had revealed the dependency of the collection coefficient on the droplets and the obstacle size, on the airflow velocity and on the location of the impinging droplets on a cylinder surface, which is determined by the angle θ between the radius vector to

the point of impingement on the surface and the x-axis of the cylinder. This angle determines the local rate of icing in the correspondent area on the cylinder. Most often at the stagnation line ($\theta = 0$) the local rate of icing is highest. The maximum value $\theta = \theta_m$ represents the point, beyond which no particles may be deposited. The total deposition coefficient E_m is defined as the rate of deposition between the angels - θ_m and + θ_m. In a study about dusty gases (Saffman 1962, Michael 1968, Michael and Norey 1969) a concept for a "relaxation time" τ was set up as

$$\tau = \frac{2\rho r^2}{9\mu_a}, \tag{2.6}$$

defined as the time for which a droplet adjusts to the changes in the air velocity. If τ is high the droplet moves with its initial velocity and the probability to strike the obstacle surface is high. If τ is low the droplet trajectories follow the streamlines around the obstacle.

The critical value for the droplets radius r_{cr}, below which no impinging on the obstacle is possible depends on the airflow characteristics and the dimension of the obstacle. Gluchov (1989) calculates this value with the formula

$$r_{cr} = \sqrt{\frac{Stk_{cr}\mu D}{2\rho_d V_\infty}}, \tag{2.7}$$

where Stk_{cr} is the critical Stokes number, D is the dimension of the object, ρ_d is the density of the droplets and V_∞ is the velocity of the free air flow.

It should be noted that these results are mainly derived for fog droplets and rain drops. The motions of snowflakes have not been studied so extensively until now.

The most important characteristics of the icing particles, which may influence the deposition coefficient, are their sizes, the drag coefficients and their terminal velocities. These characteristics are briefly described below.

2.2.1.1 Fog droplets

It was shown by Clift et al.(1978) that the drag coefficient C_D for water droplets is similar to that one for rigid spheres up to values of Reynolds number 10^3. That is why C_D can be replaced by the experimental formula after Morsi and Alexander (1971) for rigid spheres

$$C_D = k_1 + \frac{k_2}{\mathrm{Re}_d} + \frac{k_3}{\mathrm{Re}_d^2} \tag{2.8}$$

where k_1, k_2 and k_3 are functions of the local droplet Reynolds number. They are tabulated for values of $\mathrm{Re_d}$ up to 10^5. Some of these values are given in the following Table 2.1.

Table 2.1: Values of k_1, k_2 and k_3 in Eq.(2.8)

Range	k_1	k_2	K_3
$Re_d < 0.1$	0	24	0
$0.1 < Re_d < 1$	3.69	22.73	-0.09
$1 < Re_d < 10$	1.22	29.17	-3.89
$10 < Re_d < 102$	0.62	46.50	-116.67
$102 < Re_d < 103$	0.36	98.33	-2778.0

In the following Table 2.2, composed after Mason (1957), some characteristic data about cloud droplet radii are presented.

Table 2.2: Characteristic data of cloud droplet radius after Mason (1957)

Cloud type	Number of droplets in cm^3	droplets radius, µm			Source
		Mean	median	lowest and highest	
Cumulus humilis	300	9	6	3 - 33	AufmKampe (1956)
Cumulus humilis	-	-	3.5	1 - 10	Diem (1948)
Cumulus cong.	64	24	6	3 - 83	AufmKampe (1956)
Cumulus cong.	150-600	-	5.5	2 - 40	Zaitsev (1948)
Cumulonimbus	72	20	5	2 - 100	AufmKampe (1956)
Stratocumulus	350	4	3.5	1 - 12	Diem (1948)
Stratocumulus	310	8	-	-	Bricard (1943)
Altostratus	450	5	4.5	1 – 13	Diem (1948)
Nimbostratus	330	6	4	1 – 20	Diem (1948)
Stratus	260	6	4	1 – 22	Diem (1948)

2.2.1.2 Freezing rain droplets

The rain droplets are of an order of magnitude bigger then the cloud droplets and have fall velocities between 3 and 7 m/s. For freezing rain events it is not reasonable to apply the results of Langmuir and Blodgett (1946) for in-cloud icing because in this case the gravitational term in the equation for droplets motion must be included. Best (1950) suggests Eq.(2.9) for the end velocity of raindrops falling through a standard atmosphere (20°C, 1013 hPa) at surface level

$$v_T = A(1 - \exp(-d/a)^n) \tag{2.9}$$

For a droplet radius distribution in the interval [0.3; 6.0] mm Best (1950) proposed for the constants in Eq.(2.8) $A = 932$, $a = 1.77$ and $n = 1.147$.

2.2.1.3 Snowflakes

Cornford (1965) was the first in defining the aerodynamic drag coefficient for a disc sized snowflake with diameter d_f. A correlation for the drag coefficient as a function of Reynolds numbers $\mathrm{Re}_f \in \{138;2440\}$ was found by Souster (1979). Skelton and Poots (1991) expanded the formula for values of Re_f below 138 and above 2440

$$C_D \mathrm{Re}_f = \begin{cases} \left(1 + 7.696\times10^{-3}\,\mathrm{Re}_f\right)\dfrac{64}{\pi}, & \mathrm{Re} \in [0;138] \\ \sum_0^6 \alpha_p \left(\mathrm{Re}_f\right)^{p+1}, & \mathrm{Re}_f \in [138;2440] \\ 0.2196\,\mathrm{Re}_f, & \mathrm{Re}_f > 2440 \end{cases} \tag{2.10}$$

with the coefficients α_p given by Souster (1979) as $\alpha_0 = 0.332$, $\alpha_1 = -2.41176\times10^{-4}$, $\alpha_2 = 3.178\times10^{-7}$, $\alpha_3 = -2.719\times10^{-10}$, $\alpha_4 = 2.394\times10^{-13}$, $\alpha_5 = -3.892\times10^{-17}$ and $\alpha_6 = 4.541\times10^{-21}$.

A formula for the terminal fall velocity of snowflakes was proposed by Langleben (1954), who measured their velocity by photographing falling snow particles

$$v_T = 2.699(d_f)^{0.2} \tag{2.11}$$

In Table 2.3 some values of the characteristics of freezing rain droplets and snowflakes as function of the precipitation rate P are presented after Poots (1996). Here P is coupled with the liquid water content and the terminal velocity in the form

$$w = P/3600\, v_T \tag{2.12}$$

Table 2.3: Characteristic values of freezing rain droplets and snowflakes after Poots (1996)

P ($\mathrm{mm(H_2O)h^{-1}}$)	Raindrops			Snowflakes		
	$\overline{r_d}$, (mm)	v_T, (m/s)	LWC ($\mathrm{g/m^3}$)	$\frac{\overline{D_f}}{2}$ (mm)	$v_T(\overline{D_f})$ m/s	LWC ($\mathrm{g/m^3}$)
0.5	0.49	3.71	0.037	0.59	1.034	0.134
1.0	0.58	4.29	0.067	0.77	1.103	0.252
1.5	0.63	4.59	0.094	0.86	1.134	0.367

2.2.2.1 Collision efficiency

The collision efficiency can be defined as the ratio of the amount of droplets which impinge on the obstacle surface to the net amount of droplets in the windward cross section of the obstacle.

For the case of a cylinder the collision efficiency can be expressed as function of two dimensionless parameters

$$K = \frac{V\rho_w d^2}{9\mu D} \tag{2.13}$$

and

$$\phi = \frac{Re^2}{K} \tag{2.14}$$

where *Re* is the droplet Reynolds number ($Re=\rho_a dV/\mu$), *d* the droplet diameter, *D* the diameter of the cylinder, ρ_w the water density, μ the absolute viscosity of the air and ρ_a the air density.

The exact formulations after Langmuir and Blodgett (1946) for the total collection efficiency E_m in case of a circular cylinder can be written as

$$E_m = 0.466(\ln 8K)^2, \quad 0.125 < K < 1.1 \tag{2.15a}$$

and

$$E_m = \frac{K}{\left(K + \frac{\pi}{2}\right)}, \qquad K > 1.1 \tag{2.15b}$$

The values of θ_m determining the maximum width of possible deposition on the surface of the cylinder are

$$\tan\theta_m = 1.70(K - 1/8)^{0.76}, \quad 0.125 < K < 10 \tag{2.16a}$$

and

$$\tan\theta_m = K \qquad K > 10 \tag{2.16b}$$

This maximum deposition area can also be expressed in terms of the so-called upper and lower grazing trajectories.

More recently Finstad et al.(1988a) examined the equation of droplet motion numerically and found the following empirical fit to the calculated data:

$$\alpha_1 = A - 0.028 - C(B - 0.0454), \tag{2.17}$$

with

$$A = 1.066K^{-0.00616}\exp(-1.103K^{-0688})$$

$$B = 3.641K^{-0.498}\exp(-1.497K^{-0.694})$$

$$C = 0.00637(\phi - 100)^{0.381}$$

Makkonen and Stallabrass (1987) carried out an experimental verification on the theoretical results of Langmuir and Blodgett (1946), investigating icing in a wind tunnel using three categories of data. They showed that the experimental data coincide excellently with theoretical results, reporting a linear correlation of 0.99 as Figure 2.2 shows.

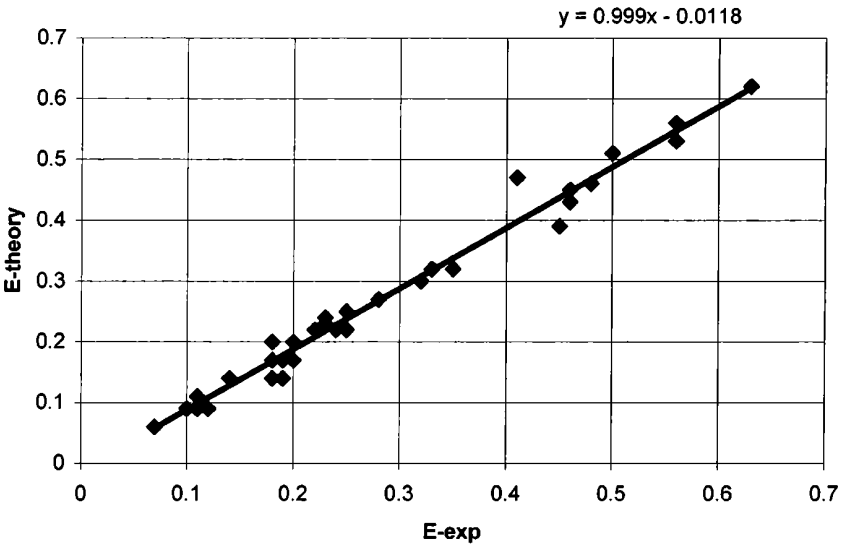

Figure 2.2: Theoretical (E-theory) and experimental (E-exp) collection efficiency of rotating cylinders; after Makkonen and Stallabrass (1987)

It should be noted that all these formulas give results for a certain droplet size d_j. For calculating the mean theoretical deposition coefficient an integration of all size categories of the droplet distribution is necessary as

$$E_{mean} = \frac{1}{w} \int_{r_{min}r}^{r_{max}} \frac{4}{3}\pi r^3 n(r) E(r) \rho_w dr, \tag{2.18}$$

where $n(r)$ is the spectral density of the droplets distribution and $\frac{4}{3}\pi r^3 n(r)dr$ the mass of water comprised in droplets with radius between r and dr.

However, for simplification, the mean collision efficiency can be determined by an approximation for monodisperse droplet size spectrum at the median volume diameter (MVD). Langmuir (1946) suggested this in his initial icing investigations on Mt. Washington. His calculations were carried out on the assumption that all the particles in a given condition with fog were of uniform size. He introduced the monodisperse droplets spectrum as the diameter (or radius) such that half of the liquid water content of the fog is comprised by droplets of larger size and the other half by smaller droplets. Beside this approximation for MVD other approaches have been used in recent years – for example the mean volume droplet diameter D_{mv} (after Prodi et al. 1986) and the mean droplet diameter D_m, defined as follows

$$D_{mv} = \left(\frac{6}{\pi} \frac{V}{N} \right)^{\frac{1}{2}} \tag{2.19a}$$

and

$$D_m = \frac{\sum_i n_i D_i}{N} \tag{2.19b}$$

Finstad et al.(1988b) could show later that the use of MVD is the best way to fit the droplet distribution. The authors calculated the MVD after Lozowski (1978) who expressed the MVD by the mean of an interpolation formula assuming a uniform droplet diameter distribution within each of N size bins with equal width W

$$\mathrm{MVD} = \mathrm{W}\left(\frac{(0.5-u_{k-1})}{(u_k-u_{k-1})}\times\left[k^4-(k-1)^4+(k-1)^4\right]\right)^{0.25}, \qquad (2.20)$$

where k is the k-th bin, u_k is a cumulative fractional volume, such that

$$u_k = \frac{1}{V}\sum_{i=1}^{k} v_i, \qquad \mathrm{u_{k-1}} < ½ \text{ and } \mathrm{u_k} > ½$$

Here V is the total volume of all droplets in all bins and v_i is the volume of water comprised in the droplets of the i-th bin. Finstad et al.(1988b) gave also a mathematical justification for the MVD approximation.

Another expression of MVD can be found according to Best (1951) who showed that the water droplet distribution could be described by the formula

$$1-F = \exp\left(\frac{-2r_d}{a}\right)^k \qquad (2.21)$$

where F is the fraction of liquid water comprised by droplets with radius $r < r_d$. The MVD is then the radius for which $F(r_d) = ½$.

2.2.2.2 Sticking efficiency

This coefficient can be defined as the ratio of the number of droplets, which strike the surface of the obstacle (and thereafter may bounce from there) to the number of droplets remaining on the surface. This efficiency depends on the liquid water content in the particles, their impact velocity and temperature, as well as on water-phase mixture on the ice-accreting surface. The liquid water droplets generally do not bounce. In these cases α_2=1.

When the icing particles are snowflakes the bouncing is very effective. Wakahama et al.(1977) proved this by photographing snow particles, showing up to 80% of them bouncing. The sticking efficiency for the snow particles depends on their water-phase mixture. If the snow particles are completely solid (dry snow), α_2 is close to zero. If there is a liquid layer on the snow particles (wet snow), the sticking efficiency approaches unity.

Until today the sticking efficiency for wet snow has still not been sufficiently investigated. There are only empirical equations. The approximation for α_2 for a cylinder mostly used now is (Admirat et al.1988)

$$\alpha_2 = \frac{1}{V}, \qquad (2.22)$$

where V is the wind speed (m/s) and α_2 is close to 1 at low wind speeds.

2.3 Dry and wet growth regimes

According to the ice accretion regime, an icing process can develop by two different mechanisms, namely dry and wet growth.

The theoretical investigations of Schumann (1938) and Ludlam (1950, 1951, 1958) showed that the temperature of an ice deposit being formed by the freezing of super cooled droplets increases above the temperature of the surrounding air mass due to the release of heat from fusion. This was also experimentally confirmed by Melcher (1951) and Macklin (1962). The temperature of the deposit is determined by the heat balance of the ice surface and the impinging droplets. Because the deposit temperature cannot exceed 0°C, there is for a given ambient temperature, wind velocity and dimension of the obstacle a critical liquid water content for which all incoming water could freeze. If the liquid water content is above the critical value the excess water cannot freeze and is incorporated into the ice structure in form of spongy ice deposition. Ludlam (1958) classified these mechanisms as dry and wet growth regimes.

2.3.1 Dry growth regime

In the dry growth regime all impinging water freezes. The heat released during freezing of a droplet is carried out before another droplet arrives. The temperature of the deposit in this case is below 0°C, which allows transfer of heat on to the surface. Macklin et al. (1968) defined three phases of freezing – the initial freezing, the subsequent freezing and the cooling phase. The initial freezing occurs when a droplet arrives on the surface, a fraction of the droplet freezes at the expense of the remaining amount, which increases its temperature. The subsequent freezing is controlled partly by heat conduction into the surface and partly by forced convection and evaporation to the surrounding. When the freezing process is completed the cooling phase begins. Macklin and Payne (1968) examined these freezing times as well the depth of penetration. At lower temperature in this regime the smaller droplets freeze quasi-instantly with air bubbles between them. The structure of the deposit then is porous and opaque.

2.3.2 Wet growth regime

Wet growth of ice deposition occurs when the droplet freezing time is sufficiently long and the released heat of fusion cannot be carried out from the surface. The surface temperature rises towards 0°C and there can be no flow of heat into the deposit. In this case liquid water is entrapped in the ice deposit (Knight 1968, Blackmore et al. 2002). The structure is spongy transparent or clear ice.

2.3.3 Critical conditions

The critical conditions that separate dry growth and wet growth are characterized by the values of the factors governing the icing on an object (droplets diameter, dimension of the object, liquid water content, wind speed, air temperature). Thus, it is important to know the thresholds of these values at which this change occurs. These were investigated and presented by Mazin (1957) and Makkonen (1981).

Mazin's formula for the critical water content W_{cr} is given by

$$W_{cr} = \frac{k_a\left(-t_a + \frac{0.628L_e(e_o - e_a)10^{-3}}{c_p p_a} - \frac{\mu V^2}{0.01 I_m c_p}\right)}{EV(80 + t_a + \frac{V^2}{2I_m})10^6} \tag{2.23}$$

Makkonen found the following formula

$$W_{cr} = \frac{k_a}{E}\left(\frac{\rho_a}{VD\mu_a}\right)^{\frac{1}{2}} \frac{-t_a + \frac{kL_e}{c_p p_a}(e_o - e_a) - \frac{rV^2}{2c_p}}{L_f + c_\omega t_a} - \frac{\sigma n' t_a}{Ev(L_f + c_\omega t_a)}, \tag{2.24}$$

where in both equations k_a is the molecular thermal conductivity, D the dimension of the object, I_m the mechanical heat equivalent, $k = 0.62$, L_e the latent heat of evaporation, L_f the latent heat of freezing, e_o and e_a the saturation vapour pressures over water at 0°C and at t_a, respectively, p_a the atmospheric pressure, c_p the specific heat of air at constant pressure, c_w the specific heat of water, here r is the recovery factor for viscous heating, v the wind velocity, σ the Boltzmann constant and $n' = 8{,}1.10^7 K^3$ the radiation linearisation constant. Here E should be understood as the product of the collision and sticking efficiency i.e. $E = \alpha_1 \alpha_2$

2.4 Accretion efficiency

The coefficient accretion efficiency α_3 (c.f. Eq.2.3) can be defined as the part of the deposited supercooled water droplets that accretes as ice on the surface of the object. This coefficient is different for the different icing regimes. In the dry growth regime, as mentioned above, all the impinging droplets freeze and the accretion efficiency is unity.

In the wet growth process the heat balance of the surface does not allow the release of the latent heat of freezing of a droplet before the arrival of the next droplet. Hence not all droplets can be frozen. One part of the liquid water runs off from the surface and the other part remains there. A water film develops on the surface of the obstacle. In this regime the ice accretion rate is determined by the heat balance of the icing surface.

2.5 Heat balance of the icing process

Heat balance investigations of the icing process have been made by many researchers (Messinger, 1953, Lozowski et al.1983; Cansdale and Gent 1983; Makkonen 1984; Jones 1996; Mazin et al.2000). The mathematical form of the heat balance equation for an ice-accreting surface can be taken after Makkonen (2000) as follows

$$q_f + q_v = q_c + q_e + q_l + q_s, \tag{2.25}$$

where q_f is the latent heat released at freezing, q_v the aerodynamic heating of air, q_c the heat loss to the air, q_e the heat loss of evaporation, q_l the heat loss due to the warming of the deposited

liquid water to the freezing temperature and q_s heat loss due to radiation. The calculation of the terms in Eq.(2.25) can be done as follows

$$q_f = I L_f, \tag{2.26a}$$

where L_f is here the latent heat of fusion and I is the intensity of ice accretion.

In case of wet growth q_f is

$$q_f = (1-\lambda)\alpha_3 F L_f, \tag{2.26b}$$

where λ is the liquid fraction of the accretion for which 0.3 can be assumed and F is the water flux density.

In a wet growth regime the heat conduction into the ice deposit is negligible and because the kinetic heating of air q_v is small it can be also neglected.

The convective heat transfer is given by

$$q_c = h(t_s - t_a), \tag{2.26c}$$

where h is the convective heat-transfer coefficient and t_s is the temperature of the icing surface (t_s=0°C at wet growth process).

The evaporation heat transfer is

$$q_e = 0.622\, h L_e \frac{(e_s - e_a)}{c_p p}, \tag{2.26d}$$

where L_e is the latent heat of vaporization, e_s is the saturation water vapour pressure over the accretion surface and e_a is the ambient vapour pressure.

The term q_l can be written as

$$q_l = F c_w (t_s - t_d), \tag{2.26e}$$

where c_w is the specific heat of water and t_d is the temperature of the droplets at impact.

The last term is

$$q_s = \sigma n'(t_s - t_a), \tag{2.26f}$$

where σ is the Stefan-Boltzmann constant and n' is again the radiation linearisation constant. Here only the long-wave radiation is considered because in icing conditions solar radiation is negligible.

From the equation of the heat balance Makkonen (2000) deduced the formular for the expression of the accretion efficiency α_3.

2.6 Density and structure of the icing depositions

As mentioned before the structure and the density of the ice accreted on an object depends on the meteorological conditions, the properties of the droplets and the thermal conditions during the

process. The ice depositions vary in different forms and structures and have also a wide range of density (from about 0.1 to 0.9 g/cm^3).

It has been found that the density increases with increasing wind speed, ambient temperature, droplet diameter and the liquid water content, and decreases with increasing size of the obstacle (Langmuir and Blodgett 1946, Macklin 1962). Macklin found that the density could be expressed as a function of the mean temperature T_s of the ice accreted surface and the product of the median droplet volume radius and the impact speed, rV_o, and suggested the following formula for this relationship

$$\rho = 0.110 \left(-\frac{rV_o}{T_s} \right)^{0.76}, \tag{2.27}$$

where ρ (g/cm^3) is the density of the deposited rime ice, r (μ) the median volume droplet radius and V_o the impact velocity (the velocity with which the droplets impinge on the surface of the obstacle). The term $R \equiv -(rV_0/T_s)$ is now known as the *Macklin parameter*.

The dependence on the temperature is more complicated at higher temperatures. At temperatures below –20° C Macklin found that the density becomes independent of the surface temperature and depends only on rV_o. This is expressed by the following formulae in terms of Macklin's parameter:

$$\rho = 110\ R^{0.76}\ (\text{kg/m}^3), \qquad R \leq 17$$

$$\rho = 917\ (\text{kg/m}^3), \qquad R > 17$$

In order to give a physical interpretation of this relationship Macklin investigated the internal structures of the ice depositions formed under various conditions. He found that at temperatures below –16°C the droplets freeze individually, even at high impact speeds, if they are packed very closely. If the impact speed is low and the freezing time is short, the droplets retain their spherical shape and form an open structure with entrapped air and low density. If the speed is higher and freezing time longer the impinged droplets are more closely packed and the density is higher. With increasing temperature the droplets begin to merge but individuals can still be distinguished. At temperatures close to 0°C the droplets are fused together without distinguishable individuals. The ice structure in these conditions is clear ice without entrapped air and the density is very high. This amalgamation of the droplets may be due to two physical processes, namely the spreading of liquid water across the underlying surface layer and their partial or complete coalescence before they freeze. The second reason is less likely because the freezing time of the individual droplets is too short (Macklin 1962).

The freezing rate of an accreted droplet is limited by the rate of heat transfer to the environment. The temperature of the droplet will rise to 0°C during the freezing process because the heat of fusion cannot be dissipated rapidly enough. It is likely that freezing of a drop begins from outside inwards building a thin ice layer on the surface. This outer shell develops because the heat of freezing is most readily conducted away through the surface layer of the droplet. Further, because the thermal conductivities of water and ice are considerably higher than that for air, transfer of heat first takes place rapidly between the droplet and the ice surface.

The main factor for the fusion of the droplets and the increase in density is the spreading of the droplets. This effect also increases with increasing temperature which has been reported by many authors (Dufor 1861, Weikmann 1953). So Weikmann reported that below –5°C droplets solidified individually, whereas at higher temperatures they spread over the ice surface and

spongy ice is formed. Below –14°C all droplets of up to 150 μ radius solidified as spheres, whereas at –5°C most of them were flattened. Macklin (1962) examined theoretically the density of ice depositions by assuming that the droplets freeze as spheres of density 0.9 g/cm^3. He found that the maximum density of an ice deposition in this case could not exceed 0.67 g/cm^3 and densities above 0.7 must be due to distortion and spreading of the droplets. As an explanation for his empirical discovery Macklin stated that the density of an ice deposition depends on the impact momentum of the impinging droplets and the surface temperature of the obstacle. If the surface temperature is low and the impact velocity of the droplets and their radius are not high this will permit a quick freezing of the droplets as spheres on the surface of impact. In this case the droplets freeze individually and the structure of the deposition is fragile. In the opposite case (temperature close to 0°C, higher wind speed and droplet radius) the freezing rate is not high and the binding force between the arrived droplet and the surface is not sufficient to overcome the impact momentum of the droplet and it begins to spread. Now the structure of the deposit is much more compact and transparent or clear.

To evaluate this phenomenon Macklin (1968) introduced the spreading factor S, defined as

$$S = \frac{final.diameter.of.the.frozen.droplet}{initial.diameter.of.the.droplet} \tag{2.28}$$

Makkonen and Stallabrass (1984) derived from wind tunnel experiments the following best-fit equation for the density of rime ice in terms of Macklin parameter R:

$$\rho = 0.378 + 0.425(\log R) - 0.0823(\log R)^2 \tag{2.29}$$

They concluded that the difference between the ice densities given by Eq.(2.29) and the original Macklin formula is due to errors in the droplet size measurements by the oil-slide method, used by Macklin. Many other investigations of the density of ice have been reported as those by Jones (1990), Prodi et al. (1986) and Levi et al.(1991).

3. Modelling of icing processes

Icing is a meteorological phenomenon that can cause high ice and wind loads on structures. A good icing model describing these effects allows not only the mathematical formulation of the processes, but also the quantitative estimation of the ice mass, on the basis of available meteorological data. Because of the rare availability of icing measurements, this is often the only possibility to assess the icing potential for the place of interest. If an object is equipped with a de-icing system it is also important to know when icing may occur. In recent years considerable progress in this field has been made.

The physical parameters governing the process of icing (wind speed, temperature, liquid water content, density of the deposition, dimension of the object, structure of the accreting ice surface, droplet sizes, as well as some characteristics included in the heat balance equations) change with time. When reaching the critical conditions the process transforms from dry to wet growth regimes or vice versa and this should be also foreseen in the model scheme.

The regime of dry growth is easier to describe, because all the impinging droplets freeze quasi-instantly at the point of impact. The intensity of the dry process is however very sensitive to the droplet diameter and liquid water content, which is not the case in the wet growth regime (as shown by Makkonen 1981). Thus the MVD and liquid water content should be determined very precisely particularly for rime ice.

Another important factor is the dependence of the collision and sticking efficiencies on the form of the obstacle. Their local values around the surface determine the shape of the deposition. The modelling of wet growth process is more complex because of the persistence of unfrozen water, the properties and location of which have to be taken into account in the local heat transfer analysis. The wet process and real shape of the deposition can be calculated and simulated determining the local coefficients of collision, sticking and accretion as well as the local heat balance equations (Lozowski et al.1983, Makkonen 1985, Poots 1996).

Such precise calculation of the icing shape is of great importance in applications where the aerodynamical influences have to be considered. This is typical for icing of aircrafts and blades of wind turbines.

Where icing on power lines is considered, the torsion of the conductors caused by gravitational force acting on the asymmetrical deposition should be taken into account too. Low torsional stiffness tends to increase the ice loads (Popov and Holodov 1978, McComber, 1990). Sometimes in freezing rain icicles may grow which as shown by Makkonen (1998) may lead to heavy ice loads. The mechanisms of icicle growth and modelling of this process have been presented by Maeno and Takahashi (1984), Makkonen (1988) and Maeno et al.(1994).

For simplifying the models some assumptions may be applied. For example, a cylindrical form of the obstacle could be used as a first approximation to its real form. Another simplification is for the form of the deposition itself. To avoid problems with the accretion shape it may be assumed that the deposition has cylindrical geometry, which in some cases is very close to reality. This assumption has the advantage that the standards for ice loads in the design practice are given in terms of equivalent ice thickness.

In the models for rime icing the equation for the density ρ of the depositing ice or another similar relationship are used (as in the model of Stanev et al.1970).

In the models of glaze and wet snow frequently the following constant values for ρ are used, namely 0.9 g/cm^{-3} and 0.4 g/cm^{-3}, respectively.

Another empirical finding in icing modelling is for the relationship between the horizontal visibility and the liquid water content the following expression (Trabert formula, see Aufm Kampe et al., 1952)

$$Vis = Cr/w, \tag{3.1}$$

is used where *Vis* is the visibility in meters, *r* is the droplets radius (μ) and *w* is the liquid water content (kg/m^3). Kampe et al. (1952) critically investigated this formula and showed that *C* is not really a constant but depends on the droplets radius. Another approach is given farther below as Eq.(3.1a). The relationship between the visibility and liquid water content for snowfall is different and has been used to estimate the accretion of wet snow (Makkonen 1989).

3.1 Models for in-cloud icing

The intensity of an icing process is defined by the ratio of water mass flux *F* (kg/h) to the surface *A* of the obstacle as

$$F = wVA. \tag{3.2}$$

This maximum flux is reduced by influences expressed by the collision, sticking and accretion efficiencies α_1, α_2 and α_3, respectively.

In the process of in-cloud icing the dominating factor is the horizontal force due to wind velocity, whilst the gravitational term can be omitted.

3.1.1 The model of Stanev and Moraliiski

Stanev and Moraliiski (1987) and Stanev et al.(1987) developed a physical-statistical model for rime icing in the mountain regions of Bulgaria, where this type of icing is prevailing in up to 88 % of all cases. The model uses three simplifications. These are:

- a laminar airflow, which is disturbed only by the obstacle; the form of the obstacle being a circular cylinder with radius R_0;
- water droplets are spherical with constant radius and do not interact – i.e. no coagulation and sublimation is allowed, which is a reasonable assumption. For example at a given mean liquid water content of 1 g/m^3 and mean radius of droplets 5 μm the total mass of water is 10 times lower than that of the same air volume. In this case the mean distance is of magnitude 10^{-3}m and therefore the probability of coagulation is insignificant.
- the process of riming is stationary.

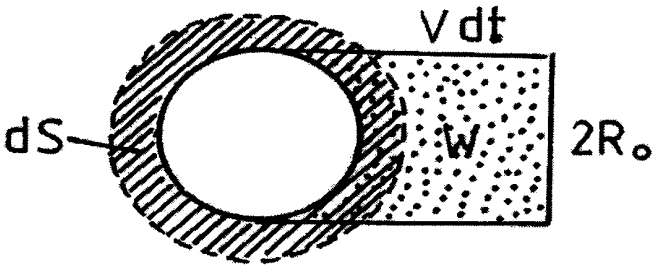

Figure 3.1: Scheme of ice growing, according to Eq.(3.3) - (3.7)

It is here assumed that the deposited ice is uniformly distributed around the obstacle. Then the deposited ice mass (Figure 3.1) of unit length of the cylinder is given by:

$$\rho dS = EwV_n 2Rdt\,, \tag{3.3}$$

where E is the collection efficiency, w is the liquid water content, ρ is the density of the deposited ice, R is the radius of the depositing ice (m), V_n is the wind velocity normal to the cylinder, dS is the change of the area of the deposition for time dt.

When replacing S with the formula for the area of the cross section of the obstacle (in this case a circle) and dS by

$$dS = 2\pi RdR \tag{3.3a}$$

and replacing this in Eq.(3.3) leads to:

$$\pi\rho(R - R_0) = EwV_n(t - t_0) \tag{3.4}$$

Taking into account the influence of the direction of the wind on the obstacle, defined by angle β between the wind direction and the axis of the obstacle as

$$V_n = V\sin\beta \tag{3.5}$$

the final expression for the radius of the deposited ice becomes

$$R = R_0 + \frac{EwV\sin\beta}{\pi\rho}L \tag{3.6}$$

where L is the total duration of the process and E is taken from Langmuir and Blodgett (1946) for a cylinder and $K>1.1$ as

$$E = \frac{K}{\left(K + \frac{\pi}{2}\right)}, \tag{3.7}$$

where K is the inertial parameter after Langmuir.

It should be noted that these results could be applied for the typical form of the deposition which is presented in Figure 3.2

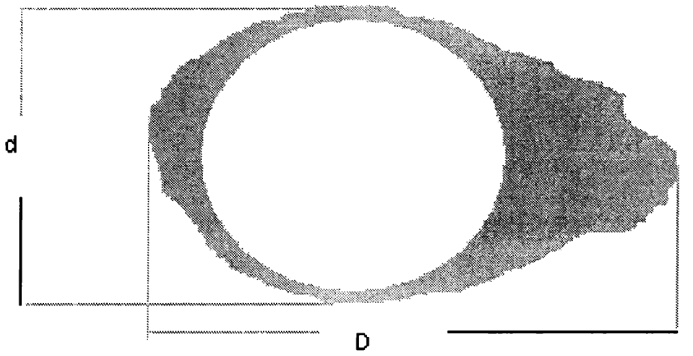

Figure 3.2: The typical form of ice deposition; D major axis, d minor axis, Eq.(3.8).

For a deposition with major axis D_{id} and the minor axis d_{id} as in Figure 3.2. from the equity of the areas of the deposition and the cross-section it follows that

$$d_{id} \times D_{id} = \pi R^2, \tag{3.8}$$

which yields equivalent results.

In this model the total duration L is then divided by N time intervals Δt_i, which coincide with the intervals for regular weather observation (e.g. 3 hours). In each interval the process is assumed to be stationary. However, because the process is very intensive initially, the fist time interval is subdivided into 6 time steps of 30 minutes each. In each time step E_i, ω_i, $V_i \sin\beta_i$ and ρ_i are calculated and their values are used as input parameters in the next time step.

$$R_i = R_{i-1} + E_i \frac{w_i V_i \sin\beta_i}{\pi\rho_i} L_i \,;\ \text{i=1,.., N} \tag{3.9}$$

Here R_0 is the radius of the cylinder at $t = 0$ and R_N will be the final radius of the deposition at t_N= N.

The mass M_i (kg/m) of the deposited ice at each time interval is then

$$M_i = \pi\rho_i\left(R_i^2 - R_0^2\right), \tag{3.10}$$

and the combined ice and wind loads F_i for the same time step results in

$$F_i = \sqrt{\left(M_i + M_o\right)^2 + Q_i^2}\,, \tag{3.11}$$

where Q_i is the wind load.

For the analogous case of a flat plate with area S it can be considered using the corresponding formulas which are respectively:

- for the thickness of the deposition:

$$h_d = E_{hi} \frac{w_i V_i \sin \beta_i}{\rho_i} \tag{3.12}$$

- for the mass of the deposited ice:

$$M_{hi} = \rho_i h_i S, \tag{3.13}$$

Because some of the parameters in the formulas are not routinely measured at weather stations the model uses three empirically found relations (Stanev et al.1987):

- liquid water content of the fog and the horizontal visibility;
- density of the depositions and the air temperature;
- droplet radius and the air temperature,

and are presented in the Figures 3.3 - 3.5.

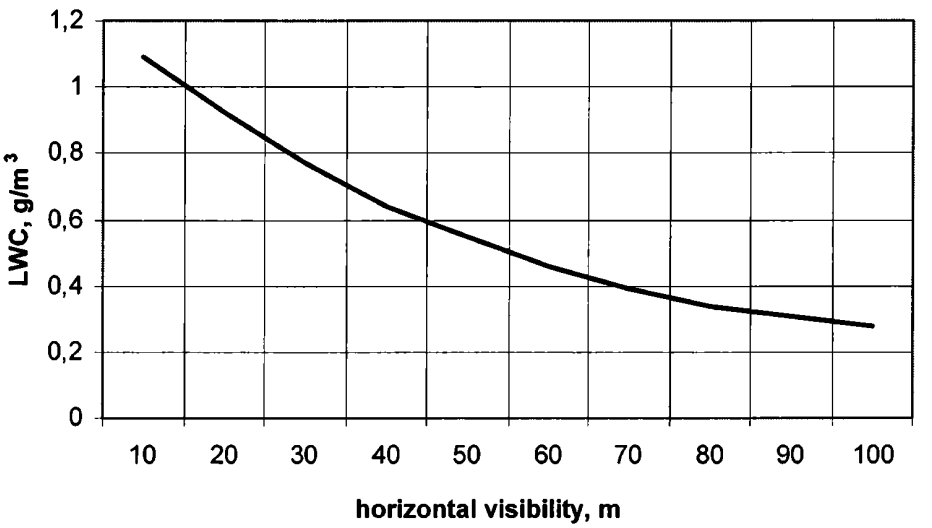

Figure 3.3: Relationship between the horizontal visibility and the liquid water content

This gives the empirical relationship between the visibility (*Vis*) and the liquid water content in the form

$$w = a \exp(-Vis/b) \tag{3.1a}$$

where a = 1,2285. 10^{-3} and b = 63.0107 with *Vis* taken in meters and *w* in kg/m^3.

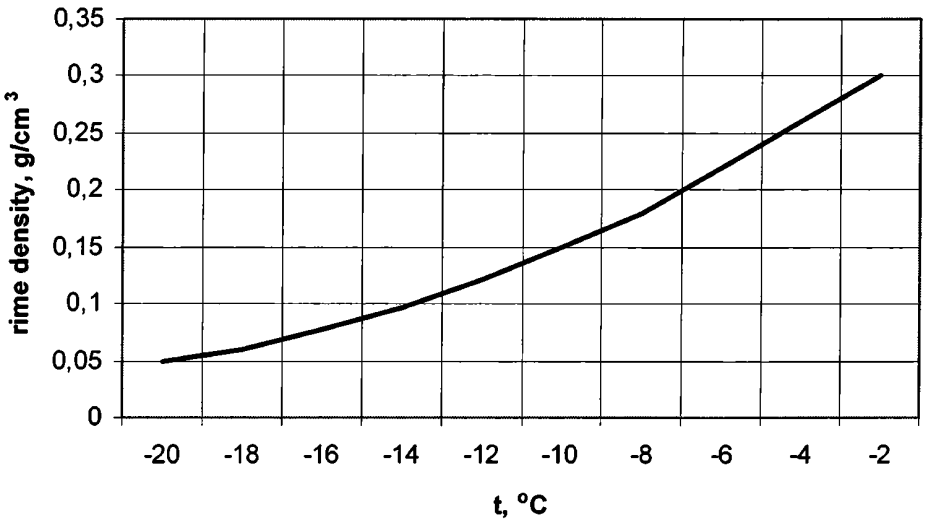

Figure 3.4: Relationship between air temperature and the density of deposition

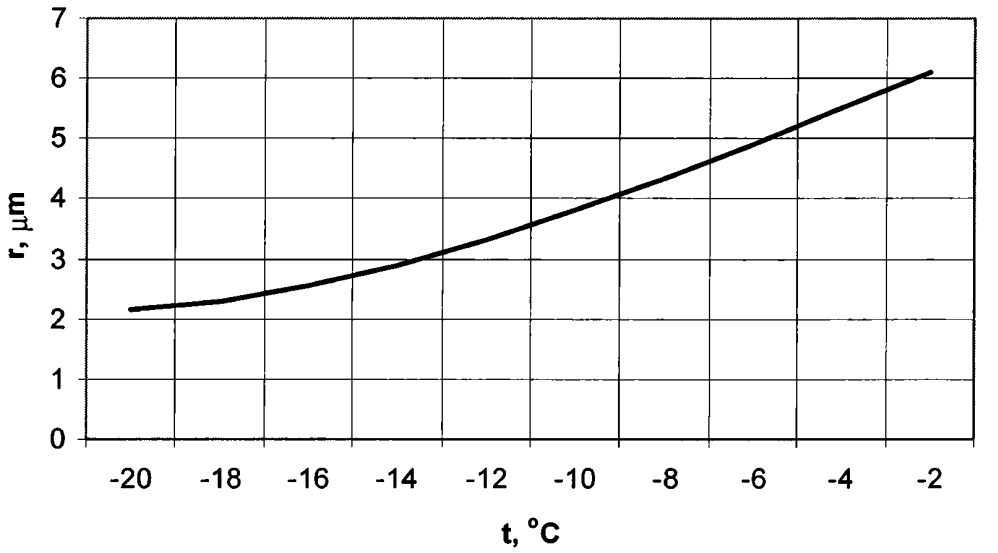

Figure 3.5: Relationship between air temperature and mean radius of the droplets

A comparison between the experimental and the theoretical values found for the radius of the deposition for examples of rime icing on peak Cherni vrach, Vitosha mountain (Bulgaria), are given in the Table 3.1.

Table 3.1: Experimental and theoretical values for the deposition radius

Date	$R_{theor.}$	$R_{exp.}$
	cm	
3.01.1970	10.5	9.9
12.11.1970	6.8	7.2
11.12.1970	8.3	8.6
2.01.1971	8.0	8.7
26.01.1971	6.5	6.9
08.01.1972	5.6	8.1
17.12.1973	12.6	11.3
02.02.1976	5.1	4.8
14.01.1977	8.2	6.7
17.03.1977	6.8	6.2

The model gives good agreement with experimental results for rime icing. It has not been adjusted yet to the wet growth process. This can be achieved by including the freezing fraction β (after Mazin 1957) or n after Makkonen (1984) or Lozowski et al.(1983).

3.1.2 The in-cloud icing model of Makkonen

The model of Makkonen was designed firstly to simulate the intensity of in-cloud icing both for dry and wet growth regimes on stationary structures of constant size and orientation (Makkonen 1981). It showed that the icing intensity in wet growth could be expressed independently from the liquid water content and collection efficiency. Later the model was adjusted as time dependent model for icing on cylindrical objects (Makkonen 1984). In the later model (known as the *cylindrical-sleeve icing model*) Makkonen examined the icing of wires perpendicular exposed to the wind vector and expressed the icing intensity I on the cylindrical surface as

$$I = \frac{2}{\pi} EnwV, \tag{3.14}$$

where E is the collection efficiency and n is the freezing factor, defined as 'the ratio of the icing to the mass flow of the impinging water droplets'.

The quantities I, E and n are given for the whole wire which is allowed to rotate for more than 360°. In the model the assumption for a circular form of deposition is adopted. This assumption is well justified in power line icing, because the asymmetric deposit of ice at the beginning of the process causes gravitational forces, which leads to twisting of the conductor. Dranevic (1971) reported elliptic depositions on transmission lines with a ratio of the minor to the major axis with 0.88 and 0.82 for glaze and rime, respectively.

Makkonen used for E in the model the empirical equation

$$E = 0.69E_m^{0.67} + 0.31E_m^{1.67}, \tag{3.15}$$

where E_m is the total collecting efficiency, calculated by using the median volume droplet diameter d_m.

The freezing factor in Eq.(3.14) was derived from the heat balance of the icing surface and is given by

$$n = \frac{\pi h}{2EwVL_f}\left[-t_a + \frac{kL_e}{c_p p_a}(e_o - e_a) - \frac{rV^2}{2c_p}\right] - \frac{t_a}{L_f}\left(c_w + \frac{\pi\sigma\, n'}{2EwV}\right)$$

where $n' = 8.1\times10^7 \mathrm{K}^3$ as in Eq.(2.26f).

This model allows for the time dependency of the parameters included in Eq.(3.16). This time dependency of the icing intensity can be expressed formally as

$$I(t) = \frac{2}{\pi}E(t)n(t)wV \tag{3.16}$$

The icing mass of unit length for time t is then:

$$M = \int_0^\tau I(t)\frac{\pi}{2}D(t)dt = wV\int_0^\tau E(t)n(t)D(t)dt \tag{3.17}$$

In each time step the ice mass M, the icing intensity I, the diameter of the deposited ice mass D, the collection efficiency E, the freezing fraction n, the density of the accreting ice ρ and the density of the total deposit $\bar{\rho}$ (see Eq.(3.21)) are calculated, using different time steps. However Makkonen showed that there is no significant difference in the results when using other time intervals. The differences are larger only at the beginning when the process is very intensive.

The ice mass at $t = t_i$ is

$$M_i = M_{i-1} + I_{i-1}\frac{\pi}{2}D_i\Delta\tau \tag{3.18}$$

and the diameter of the deposit is

$$D_i = \left[D_{i-1}^2 + \frac{4(M_i - M_{i-1})}{\pi\rho_i}\right] \tag{3.19}$$

The density of the accreting ice is calculated by using the Macklin parameter R (= - $v_0 d_m/2t_s$, see paragraph 2.6). The droplet impact speed v_0 can be obtained from the numerical solution of the equations for droplet motion. In the model an empirical fit to the data of Langmuir and Blodgett (1946) is used as

$$v_o = v(-0.174 + 1.464K_0 - 0.816K_0^2) \qquad \text{for } \mathrm{K_0} \le 0.55 \tag{3.20a}$$

and

$$v_o = v\left[0.561 + 0.592 \log K_0 - 0.26(\log K_0)^2\right] \quad \text{for } K_0 > 0.55 \tag{3.20b}$$

The surface temperature t_s in the Macklin parameter can be derived from the heat balance equation.

The total density of the deposition for time step *i* is:

$$\overline{\rho_i} = \frac{4M_i}{\pi\left(D_i^2 - D_0^2\right)} \tag{3.21}$$

The model results show that the process may change from one regime to the other under constant meteorological conditions and that the density of the ice deposit usually decreases with time. It shows further some other dependencies of the icing intensity, revealed earlier by Makkonen (1981), namely that the intensity is in general dependent on the air temperature in the wet growth process, whilst in the dry regime there is no significant dependency. The icing intensity in the dry process is proportional to the liquid water content. Changes in the droplet diameter influence the icing rate significantly.

The time dependency of the model allows the influence to be assessed of increasing the obstacle dimension of the freezing fraction, the collection efficiency and the heat balance and consequently the icing growth rate and density of the deposition. The model encounters a maximum value of the diameter D_m, which corresponds to the maximum icing rate. After reaching this diameter the icing intensity decreases.

3.1.3 The axial-growth model

This model (Lozowski et al.1983) considers icing of an unheated non-rotating cylinder perpendicular to the air stream in both dry and wet regimes. The thermodynamic conditions and the initial icing rate, influenced by the runback of unfrozen water are calculated as a function of the angle of the windward obstacle surface. For a definitive result the shape and the total mass of the deposited ice are simulated as follows.

Given an unheated and non-rotating cylinder with diameter D in a perpendicular air flow with speed v (m/s) the model calculates in a first phase the local flux of impinging super cooled droplets as a function of the position of impingement on the cylinder surface. This is made by dividing the upwind surface of the cylinder into i (i = 0,1,...18) angular sectors with 5° width each and the droplet size spectrum into nine diameter categories each 5 μm wide. The droplets in a category are assumed to have the same radius. The model calculates the collision efficiency for each angular sectors and droplet size categories, which is defined as the local collision efficiency $\beta_{ij} = \beta_j(\theta_i)$. The overall collision efficiency for each sector is the mass-weighted mean for all droplet size categories.

$$\beta_i = \beta(\theta_i) = \sum_j f_i \beta_{ij} = \sum_j f_i \beta_j(\theta_i), \tag{3.22}$$

where f_i is the part of the total water mass flux, comprising droplets in the j-th category.

The total collision efficiency for the cylinder surface is calculated then by integrating β_i for each angular sector.

For the determination of $\beta_j(\theta_i)$ the authors used the following calculation procedure. Firstly they re-examined the results of Langmuir and Blodgett (1946) and the conclusions of Oleskiw (1981) for the droplets motion and suggested a modified formula for the Langmuir inertia parameter K, which is calculated for each droplet category j. For the stagnation line ($\theta = 0$) the formula is

$$K_{0j} = 0.125 + \frac{(K_j - 0.125)}{1 + 0.0967\,\mathrm{Re}_j^{0.6367}}, \tag{3.23}$$

where $\mathrm{Re_j}$ are the Reynolds numbers and K_j are the Langmuir inertial parameters for the droplets of the j-th category. Then the values of the stagnation line collision efficiency β_{0j}, the total collection efficiency E_j and the maximum impingement angle θ_{mj}, all for the j-th droplet category, are calculated as

$$\beta_{oj} = E_j = \theta_{mj}, \qquad K_{0j} < 0.125 \tag{3.24a}$$

$$\beta_{0j} = \frac{1.4(K_{0j} - 0.125)^{0.84}}{1 + 1.4(K_{oj} - 0.125)^{0.84}}, \quad 0.125 \le K_{0j} \le 7.5 \tag{3.24b}$$

$$\beta_{oj} = \frac{K_{0j}}{1 + K_{0j}}, \qquad 7.5 \le K_{0j} \tag{3.24c}$$

$$E_j = 0.489(\ln 8K_{0j})^{1.978}, \qquad 0.125 \le K_{0j} \le 0.9 \tag{3.25a}$$

$$E_j = \frac{K_{0j}}{\frac{\pi}{2} + K_{0j}}, \qquad 0.9 \le K_{0j} \tag{3.25b}$$

$$\theta_{mj} = \tan^{-1}\left[1.7(K_0 - 0.125)^{0.76}\right], \quad 0.125 \le K_{0j} \le 10 \tag{3.26a}$$

$$\theta_{mj} = \tan^{-1} K_{0j}, \qquad 10 \le K_{0j} \tag{3.26b}$$

The empirical results of the procedure coincide very well with those of Langmuir and Blodgett (1946).

Finally the calculations for $\beta_j(\theta_i)$ were made by the following empirical formula:

$$\beta_j(\theta_i) = \beta_{ij} = \beta_{0j}\cos\left(\frac{\pi}{2}\frac{\theta_i}{\theta_{mi}}\right) + \frac{\pi^3}{\theta_{mj}^3(\pi^2 - 4)}\left(E_j - \frac{2\theta_{mj}\beta_{0j}}{\pi}\right)\theta_i^2 \sin\left(\pi\frac{\theta_i}{\theta_{mj}}\right), \quad \theta_i < \theta_{mj} \tag{3.27a}$$

and

$$\beta_j(\theta_i) = \beta_{ij} = 0 \qquad \theta_i > \theta_{mj} \tag{3.27b}$$

These formulas satisfy the physical constraints $\beta_j(0^o) = \beta_{oj}$, $\beta_j(\theta_{mj}) = 0$ and

$$\int_0^{\theta_{mj}} \beta_j(\theta) d\theta = E_j$$

The second part of the model considers the heat balance of the icing surface. The new approach allowed the influence of the moving unfrozen water to be included. Neglecting the radiative heat flux between the accretion and the air flow and the heat flux between the accretion and the underlying surface, the authors gave the heat balance equation in the form (Messinger, 1953):

$$q_c + q_e + q_v + q_k + q_f + q_w + q_w^* + q_f^* = 0 \tag{3.28}$$

Here the indices are the same as in (Eq. 2.25), q_w^* is the heat flux between the unfrozen water and the underlying accretion and q_f^* is the latent heat of flux liberated by freezing a part of or all the runback unfrozen water. This equation was applied for each angular sector, starting from the stagnation line outwards to $\theta = \pi/2$, taking into account that half of the runback water from the first sector flows downward around the cylinder surface. The runback water does not affect the heat balance of the sector of departure, but influences the sector where it goes.

The heat flux of the unfrozen water in the new sector is given by

$$q_w^* = R_w^* \overline{c_w}(t_s^* - t_s), \tag{3.29}$$

where R_w^* is the runback mass flux in the new sector, t_s^* is the temperature of the runback water. However if the underlying layer is also liquid this term will be zero, because $t_s^* = t_s = 0°C$.

The latent heat of freezing of the runback water is

$$q_f^* = R_w^* I_f n \tag{3.30}$$

This detailed mass and heat transfer analysis allowed the authors to derive formulas for the icing flux in the i-th sector (R_i) and the local thickness in the same sector (h_i):

$$R_i = n_i(R_{wi} + R_{wi}^{*)} \tag{3.31}$$

$$h_i = \frac{2R_i \delta t / \rho_i}{1 + \left(1 + \dfrac{4R_i \delta t}{\rho_i D_c}\right)} \tag{3.32}$$

where n is the freezing fraction, ρ the density, R_w is the droplet mass flux, R_{wi}^* is the runback mass flux and the index i is used for designation for the i-th sector.

The model prediction of icing profiles, using the initial rate of icing on different sectors, gives good results in comparison with experimental data. While the prediction of the dry process is adequate for wet growth the differences from the experimental data are significant. The authors themselves suggested some improvements, as for example the inclusion of the time dependent effects.

3.2 Freezing rain models

The form of the depositions in freezing rain conditions depends on the diameter and the shape of the obstacle, the precipitation rate, the wind speed and the freezing rate of the deposited water. Usually asymmetrical compact depositions with or without icicles are formed. In the model of Makkonen (1998) the assumption for a uniform shape of the deposition is applied and the icicles are modelled separately.

In contrast to the in-cloud icing, the freezing rain icing events are determined mainly from the gravitational fall of the rain or drizzle droplets. Some theoretical considerations will be given below for the possible approaches applicable for this type of icing.

It is assumed that rain drops fall vertically if there is no wind. The total mass of the falling raindrops across a 1 cm^2 horizontal surface per second can be expressed (Matveev 1984) as

$$M = \frac{4}{3}\pi N \rho_d \int_{r_{min}}^{r_{max}} r^3 f(r)\, v_T(r)\, dr \,, \tag{3.33}$$

where N is the total number of droplets in $1cm^3$, ρ_d is the density of the droplets, $f(r)$ is the distribution function of the droplets radius and v_T is the end velocity of the droplets.

Then the intensity of icing I of a cylinder with radius R will be:

$$I = \frac{8}{3}\pi N \rho_d R \int_{r_{min}}^{r_{max}} E(R,r)\, n(R,r)\, r^3 f(r)\, v_T(r)\, dr \tag{3.34}$$

where E is the collision efficiency and n is the accretion efficiency.

For convenience N can be substituted with the liquid water content w. The latter is given by

$$w = \frac{4}{3}\pi \rho_d N \int_{r_{min}}^{r_{max}} r^3 f(r) dr \tag{3.35}$$

Then I becomes

$$I = \frac{2wR \int_{r_{min}}^{r_{max}} E(R,r)\, n(R,r)\, v_T(r)\, r^3 f(r)\, dr}{\int_{r_{min}}^{r_{max}} r^3 f(r) dr} \tag{3.36}$$

This integral can be solved numerically. For simplification it can be assumed, that all rain droplets collide with the cylinder surface and that all impinging water freezes (i.e. $E = 1$ and $n = 1$), hence I can be written as

$$I = \frac{2wR \int_{r_{min}}^{r_{max}} r^3 f(r) v_T(r) dr}{\int_{r_{min}}^{r_{max}} r^3 f(r) dr} \tag{3.37a}$$

or

$$I = 2wRv_T \tag{3.37b}$$

The icing intensity can also be expressed in terms of the intensity of the rain P, which is

$$P = \frac{4}{3}\pi N \int_{r_{min}}^{r_{max}} r^3 f(r) v_T(r) dr \tag{3.38}$$

Then for I follows

$$I = \frac{2\rho_d RP \int_{r_{min}}^{r_{max}} E(R,r) n(R,r) r^3 f(r) v_T(r) dr}{\int_{r_{min}}^{r_{max}} r^3 f(r) dr} \tag{3.39a}$$

and again, if E and n are unity, then

$$I = 2\rho_d RP \tag{3.39b}$$

The mass of the deposited ice after time t is:

$$M = It = \rho_d DP = wDv_T t \tag{3.40}$$

with $D = 2R$ the diameter of the cylinder.

These formulae can be used for the calculation of the icing rate and total mass of the deposit only in the case of $E = n = 1$. This can only be assumed for very small objects at low temperatures . In most cases of power line icing the first approximation ($E = 1$) is realistic for falling rain or drizzle droplets, but the second case (n = 1) is not. The droplets and the dimension of the conductors are commensurable and part of a droplet will be lost by shedding or dripping before freezing. Thus for a better assessment of the ice loads from freezing rain the heat balance of the ice accreted surface should be taken into account.

These theoretical results are also restricted to conditions with no wind. When there is wind the calculation should include also the horizontal component of the droplet motion.

3.2.1 Analytical models of icing due to freezing rain

Several simple operational models of icing due to freezing rain have been developed, and they are reviewed and evaluated by Makkonen (1998). It was concluded that other analytical models except the one by Goodwin et al. (1983) are conceptually incorrect. The Goodwin model has

been used in many instances and its results equal those of the corresponding time dependent numerical models (Makkonen 1984, 1998, Jones 1996) with the assumption of n = 1.

The basic idea is to apply Eq.(3.37b) in a more complete form, in which the drop impact speed v_i is a vector sum of the drop terminal velocity v_T and the wind speed. Using Eqs.(3.10) and (3.37b) gives

$$dR/dt = w\, v_i / \rho\, \pi \tag{3.41}$$

Integrating gives the radial ice thickness ΔR accreted in a period t

$$\Delta R = w\, v_i t / \rho\, \pi \tag{3.42a}$$

The drop impact speed is

$$v_i = (v_T^2 + V^2)^{1/2} \tag{3.43}$$

Here it is assumed that the wind is perpendicular to the cable axis. The liquid water content w can be related to the depth of the liquid precipitation H measured during the accretion time t by

$$\rho_w H = w\, v_T\, t \tag{3.44}$$

This gives for ΔR

$$\Delta R = (\rho_w/\rho)(H/\pi)\, [1 + (V/v_T)^2]^{1/2} \tag{3.42b}$$

On vertical surfaces, such as the sides of a tall mast, Eq. (3.37b) can be applied by adopting the horizontal component of the drop velocity vector only. Accordingly, Sundin and Makkonen (1998) used the following simple approach for the ice accretion intensity, namely $I = f(n, w, P)$. Setting the freezing fraction n ($0 < n \leq 1$) to unity (all impinging droplets will freeze on the surface) and using the formula for the liquid water content, they calculated the icing rate I (mm/h) using the formulation for the liquid water content w after Stallabrass (1983).

$$I = wV = 0.26\, P^{0.88} V \tag{3.45}$$

It is assumed that the collection efficiency and the freezing fraction are unity. At temperatures close to 0°C this may lead to significant errors due to runoff and icicle growth (Makkonen 1998). Theoretically, the sticking efficiency may also be less than unity because part of the accreted water in the wet process can be lost by shedding (List 1977).

3.2.2 Numerical models of icing due to freezing rain

The numerical freezing rain models proposed by Makkonen (1998) and Jones (1996) contain a model (the heat balance model) which uses the heat balance equations for calculating the ice accretion rate. Both models consider the ice accreting on a horizontal cylinder under conditions of freezing rain with a precipitation rate P (mm/h) and wind velocity V (m/s). It is assumed that the accreting ice surface has a uniform shape. In addition, in the heat balance model the water that does not freeze runs off to the bottom surface of the cylinder and may drip off or freeze as icicles. Icicle spacing is from Makkonen and Fujii (1993). The heat balance equations are similar to those used by Makkonen (1981, 1984). The temperature of the accreting ice surface is set at 0°C because the growth is assumed wet. The main difference from in-cloud icing is that the total

water flux F_{fr} (g/m^{2}s) is determined by the flux from precipitation and the flux from the wind effected liquid water content w. The total water flux to the cylinder surface is then the vector sum of these two fluxes

$$F_{fr} = \sqrt{\left(\frac{P\rho_o}{3.6}\right)^2 + (wV)^2}\,, \tag{3.46}$$

where ρ_o is the density of water. In the model w is computed using Best's formula (Best, 1950) as

$$w = 0.067P^{0.846} \tag{3.47}$$

Jones examined the magnitude of all components of the heat balance equations and omitted the viscous, kinetic and resistive heating as very small terms. The other terms determine which part of the deposited water will freeze as uniform ice deposition. The forming of icicles is initiated from "protoicicles" (Maeno et al.1994, Makkonen and Fujii 1993) and their growing rate is determined from the heat balance. The model of Makkonen (1996) includes a complete icicle growth module (Makkonen 1988, Chapter 3.2.3) and takes into account the water that is collected directly by the icicles.

3.2.3 The model of icicle growth

This model after Makkonen (1988) gives a quantitative theory of the icicle growth and can be used for estimation of the shape and the mass of the icicles. The first quantitative study of icicle growth was made by Maeno and Takahashi (1958).

Icicles form in conditions of freezing rain or melting snow at temperatures below 0°C. Icicles form from the deposited water that does not freeze on the obstacle surface. This water flows down due to the gravity, and at the bottom part of the obstacle pending drops are formed. These drops will hang on the obstacle until the gravity force overcomes the surface tension. The droplets that freeze before dripping off initiate the forming of icicles. The icicles that form firstly can be defined as proto-icicles, a stack of partially frozen hemispherical droplets with a diameter about 0.5 cm (Maeno et al. 1994).

Makkonen (1988) shows that an icicle grows as a thin ice-walled tube with unfrozen water within. The icicle growth is in two directions - in width and in length. The growth in width happens when the water freezes on the wall of the initial icicle. When all the water does not freeze on the walls a pendant drop is formed at the tip of the icicle. The growth in length occurs as a thin cover of ice growing into the pendant drop. Makkonen expresses these growths with dD_i/dt and dL_i/dt, where D is the mean diameter of the icicle and L is the length of it. He determined these terms from the heat balance of the icicle walls and the pendant drop. For the width growth he found

$$\frac{dD}{dt} = \frac{-h_w t_a + \dfrac{0.622\,L_e}{c_p p_a}\left\{e(0^\circ C) - \mathrm{Re}(t_a)\right\} - \sigma a t_a}{\dfrac{1}{2}\rho_a L_f (1-\lambda)} \tag{3.48}$$

and *dL/dt* was determined by numerical solution of the heat balance equation for the pendant drop

$$-ht_a + h\frac{0.622L_e}{c_p p_a}\{e(0^0 C) - \mathrm{Re}(t_a)\} - \alpha t_a = \frac{3.74c_w}{d^2}\left[W_0 - \pi LD\left(\rho_a \frac{1}{2}\frac{dD}{dt} + h\frac{0.622}{c_p p_a}(e(0^o) - \mathrm{Re}(t_a))\right)\right]\times \quad (3.49)$$

$$\times\left[\frac{dL}{dt} - \frac{1}{2}\frac{dD}{dt}\right]^{0.588} + \frac{2L_f \rho_i \delta(d-\delta)}{d^2}\frac{dL}{dt}$$

Here the index *w* marks the quantity for water, W_0 is the water flux to the root of the icicle, ρ_i is the density of the icicle, ρ_a is the density of the icicle walls, *d* is the inner diameter of the tube and δ is the thickness of the wall at the tip. The values for *D* in (3.51) are used from Eq.(3.50) for each time step.

The mass of the icicle is calculated by

$$M = \frac{\pi D^2}{4}\rho_a L \quad (3.50)$$

The icicle growth model has been incorporated in to the comprehensive icing model by Makkonen (1998). The model results show that at temperatures close to the freezing point, the growth of icicles can considerably increase the total ice load.

4. Meteorological parameters influencing the icing process.

The main meteorological parameters, which may influence the icing process, are the air temperature, the droplet size spectrum, the wind velocity, the liquid water content and/or the precipitation rate and the topography or the relative altitude of the place of interest. The values of these parameters vary in a wide range during an icing process. For more accurate results it is necessary to investigate the different icing types separately. The determination of the influence of only one of these parameters is hampered by the very complex interdependency between them. This is especially difficult for an event with extremely long duration when the ending and beginning of the separated processes overlap each other.

4.1 The influence of temperature

Investigations of the influence of the air temperature on icing have not revealed a strong dependency in the dry growth regime. In the case of wet growth regime there is a near-linear dependence, namely the depositing of ice mass increases in general with decreasing air temperature. In the dry growth regime the dependency is opposite but not so significant – the ice mass decreases considerably at lower air temperature (Buchinski 1969, Makkonen 1984, Gluchov 1989). The change in the accreted ice mass in wet growth is bound to the heat flux from the object to the environment, which increases when the air temperature decreases. As explained above in dry growth regime the temperature decrease is related to a decrease in the ice deposition density. Makkonen (1981) showed also that at fixed values of wind speed and air temperature the maximum icing intensity is reached in the wet process. In freezing rain the ice load may be very sensitive to the air temperature due to runoff and icicle growth (Makkonen 1998).

4.2 The influence of wind speed

The icing process depends, as mentioned before, strongly on wind speed both in dry growth and wet growth. This dependency can be formulated easier for the dry-growth process. There are many authors who have reported an empirical correlation between the icing intensity and wind speed, e.g.

Ahti and Makkonen (1982) $I = 11\times10^{-3}V$; (4.3a)

Baranowski & Lieberslach (1977) $I = 7.5\times10^{-3}V$ for soft rime and $I = 15\times10^{-3}V$ else (4.3b)

Tammelin & Säntti (1996) $I = 4.8\times10^{-3}V$. (4.3c)

These dependencies are very similar although there is obviously some influence from the local conditions of the environment (see paragraph 4.5).

4.3 The influence of liquid water content

The amount of water impinging on an object is determined by the water flux density wV. It is therefore reasonable to expect that the icing intensity is proportional to the liquid water content

until it reaches a critical value w_{cr} where transformation of the process from dry to wet regime starts. Makkonen (1981) found that in wet growth the intensity of atmospheric icing is not sensitive to changes in w.

4.4 The effect of droplet size spectrum

The effect of droplet spectrum is described mathematically in Chapter 2.2.2.1, in which the calculation of the collision efficiency is presented. As discussed, this effect can well be described by a single parameter, the median volume diameter (MVD), of the droplet size spectrum.

The effect of MVD on the collision efficiency E is very significant, so that E varies between almost zero and unity in a rather narrow range of conditions. This is particularly so, when the wind speed is small and the object size is big. Examples on this dependence can be found e.g. in Makkonen (1984).

Because MVD affects E, it also affects the limiting conditions between dry growth and wet growth and on the density of ice. When icing is wet growth, the effect of MVD is negligible.

In freezing precipitation drops are so big that E is very close to unity, so that the precipitation drop size has no direct effect on the icing rate, except on very big objects.

4.5 The influence of topography

The regional and local topography has a significant influence on the intensity as well as on the duration of an icing event. Especially in mountain areas the exposure of the slope to the prevailing wind direction is here an essential factor.

The increase of altitude intensifies the process of icing not only in mountain regions. The relative height according to the surrounding area has also a strong influence on the frequency and intensity of icing in flat areas. An increased frequency of icing events is bound to an increase in the number of foggy days with temperatures below 0°C.

Many authors have investigated this influence and some of their results are presented below. It should be noted that the derived relationships are mainly determined on the base of the local climatological and geographical conditions.

Buchinski (1969) gives the following experimentally found relation between the diameter of the deposition and relative altitude up to 300 m in the region of Donbas, Russia.

$$D = a \exp(bh), \tag{4.4}$$

where D is the mean diameter (mm), h the altitude (m) of the site and a and b are constants depending on the geographical conditions. He reported values for glaze and rime ice of a = 7.76 and 4.47, and b = 0.0032 and 0.0039 respectively. For the relative frequency of icing he found

$$P(\%) = 3.93 \exp(0.0077h) \tag{4.5}$$

For the European part of Russia Lomilina (1977) found for the coefficient K_p (which is the ratio of the icing mass P with return period of 10 years for stations in different altitudes to the icing mass P_0 with the same return period for stations in a flat area) for windward slopes

$$K_p = e^{(1.03-r)\,0.014\Delta h} \tag{4.6a}$$

and for the leeward slopes

$$K_p = 0.5e^{0.018\,(1.09-r)\Delta h} \tag{4.6b}$$

Here Δh is the relative altitude between the sites in the flat area and the location of interest and $r = n/N$ where n is the number of days with freezing rain and N is the frequency of freezing fog days and freezing rain days. The coefficient r gives a measure for the part of freezing rain in the icing events. If icing is caused by prevailing of freezing rain, then r is bigger and K_p changes less with altitude.

In ISO 12494 (2000) a formula is given for calculating a multiplying factor K_h as

$$K_h = e^{\,0.01\Delta h} \tag{4.7}$$

for ice masses at levels above terrain.

Makkonen and Ahti (1995) also found that the absolute elevation above sea level does not significantly correlate with the ice loads in contrast to the relative elevation to the surrounding terrain. They recommend for estimating the ice loads at the location of interest to use its relative height H_i, i.e. the difference between the absolute elevation of the location and the average absolute elevation of the surrounding terrain. The authors investigated the ice loads as function of the relative elevation H_i , 'the relative elevation at which certain ice loads occur' or 'rime level'. They showed that the rime level on hills is at a higher absolute altitude the higher the hill is. Ollila (1984) who analysed data of visually observed rime levels for various hills in Northern Finland obtained the following empirical formula for the rime level

$$R_{a,v} = 0.72\,H + 55\text{m} \tag{4.8}$$

where $R_{a,v}$ is the visually observed rime level and H the height of the hill above terrain.

5. Results with experimental data from Oberstrahlbach

In this paragraph the results are presented from the test site Oberstahlbach, Austria (with the coordinates 48°38´22"N, 15°07´07"E and elevation 657 m, for winter 2002/03 and 2003/4 and for comparative purposes data from Sternstein, Czech Republic (with the coordinates 48°33'35,7"N, 14°16'3,3"E, elevation 1122 m), measured only for a short period between January and April 2004. The observed icing events with all investigated cases are listed in Tables 5.1 and 5.2 showing the main characteristics of the detected icing events.

5.1 The measurements at Oberstrahlbach

The meteorological and icing data have been collected at the above described site where the following hourly meteorological data were measured at a 40 m meteorological mast with 3 levels:

- Wind speed and direction (m/s and Deg), 40 m a.g.l., 10 min. averages
  - Heated: Thies Ultrasonic 2D
  - Unheated: Kroneis 260 PL/P
- Wind speed (m/s) 20 m a.g.l., 10 min. averages
  - Heated: Kroneis 260 PRH
  - Unheated: Kroneis 260 PL/P
- Temperature (°C) I 2 m a.g.l., 10 min. averages
- Humidity (%) 2 m a.g.l., 10 min. averages
- Global radiation (W/m^2) 2 m a.g.l., 10 min. averages
- Pressure (hPa) 2 m a.g.l., 10 min. averages
- Data acquisition: Starlog 6004C
- Icing sensor hourly
- Pictures from two web cameras, one pointing to the met mast and the icing sensor the other to the rotor blades of the wind turbine, every 20 minutes

Additionally, for a rough assessment of visibility wooden white painted poles were driven into the ground at 50 m distance from each other up to a distance of 300 m from the mast within the view of one of the web cams. This arrangement was used for a rough estimation of the LWC by Eq.(3.1a).

Meteorological data were taken from the nearby located weather station Zwettl (505 m a.s.l.) of the Austrian meteorological service (ZAMG). The icing sensor, provided by the Institute of Atmospheric Research, Praha, CZ, was exposed vertically in 3 m height having 461 mm in length and 30 mm in diameter (giving an area of 0,04345 m^2) and provided hourly data for the accreted ice mass. Near this measuring site a wind turbine exists, namely a VESTAS V44/600 from which the production data were gathered hourly too.

5.2 Analysis of the collected icing data

In the Tables 5.1 and 5.2 some characteristics of the icing events in the winter months of 2002/2003 and 2003/2004 together with the average values of meteorological parameters and the ice mass at the end of the process are shown. The number of identified icing events is 35, from which 29 are in cloud icing and the rest freezing rain. It should be mentioned that probably there was an additional in-cloud icing event (from 06.02.2003 to 11.02.20003 when the wind turbine

was not in operation), but the icing sensor did not provide any data at that time. Unfortunately a lighting strike in December 2003 damaged the measuring equipment severely so that nearly two months of measurements in the central winter period 2003/2004 are missing. The full measurements programme commenced again at the end of February 2004. From the tables it can be seen that on average the icing events were rather short, mostly less than 10 hours and only 4 events with around 40 hours duration (maximum 45 hours). For the winter months of the season 2003/2004 only 11 cases of in-cloud icing have been registered (Table 5.2). From them only 4 cases are longer then 10 hours (maximum 35 hours). The maximal deposited ice masses for this season are 2,2 and 1,6 kg/m^2, whilst the maximal values caused by in-cloud icing in 2002/2003 were 12,2 and 6,0 kg/m^2. In 2004 there are only a few cases until the beginning of February and after that no icing data were available. The more significant cases in January are those on 08.01 and on 26.01. The second one gives the longest duration for 2003/04 and one of the maximal ice mass values.

Table 5.1: Icing events and their characteristics at the test site Oberstrahlbach, winter 2002/2003

Begin	End	Type	Duration hours	mean intensity gr/h	U40 mean	U20mean	mean T, °C	Humidity, %	max. ice mass, kg/m^2
20.12.02 0000	20.12.03 0900	in cloud	10	0.9	4.1	3.1	-8.9	92	0.56
20.12.02 1600	20.12.02 1700	in cloud	1	2.0	3.5	2.4	-5.5	91	0.23
23.12.02 1400	24.12.02 1600	in cloud	26	3.7	5.1	3.4	-6.5	93	4.7
25.12.02 0000	28.12.02 2100	in cloud	45	2.9	5.2	0.9	-5.8	94	12.2
31.12.03 1100	31.03.02 1200	in cloud	1	2.0	5.5	5.2	-2.5	95	0.3
12.01.03 0300	12.01.03 0800	in cloud	5	1.5	4.1	2.5	-14.4	86	0.5
14.01.03 0300	14.01.03 0700	in cloud	4	3.8	6.7	5.7	-0.7	89	0.83
18.01.03 0400	18.01.03 0500	in cloud	1	3.0	4.7	3.5	-3.7	92	0.3
19.01.03 0600	20.01.03 0400	in cloud	22	0.9	3.6	2.1	-5.6	94	1.5
20.01.03 1700	22.01.03 1000	in cloud	41	3.1	4.8	1.8	-5.0	94	6.0
02.02.03 0200	02.02.03 1000	in cloud	8	0.8	2.7	2.1	-13.7	87	0.3
17.02.03 1100	17.02.03 1300	in cloud	2	2.0	1.7	1.5	-6.2	80	0.3
18.02.03 0700	18.02.03 1000	in cloud	3	2.3	2.3	1.7	-13.5	85	0.4
20.02.03 0100	20.02.03 1200	in cloud	11	1.1	1.5	1.1	-9.2	91	0.8
21.02.03 0400	21.02.03 1100	in cloud	7	1.3	3.8	3.3	-4.7	95	0.6
22.02.03 0100	22.02.03 0800	in cloud	7	0.5	2.4	1.7	-6.7	93	0.4
05.03.03 0100	05.03.03 1100	in cloud	11	0.4	1.8	1.4	-2.5	97	0.4
22.12.02 2000	23.12.02 02.00	freezing rain	6	12.4	5.2	3.4	-1.0	98	7.6
22.01.03 1600	22.01.03 2100	freezing rain	5	2.0	1.5	1.0	-0.2	98	0.8
24.01.03 0600	24.01.03 0800	freezing rain	2	12.0	6.2	5.2	0.0	96	1.2

Table 5.2: Icing events and their characteristics at the test site Oberstrahlbach, winter 2003/2004

Beginning	Ending	Type	Duration hours	mean Intensity g/h	U40 mean	U20 mean	mean T, °C	Humidity, %	max. Mass, kg/m²
28.10.03 1900	29.10.03 1100	in cloud	16	1.2	3.6	3.1	-2.3	94	1.1
29.10.03 1400	29.10.03 2100	in cloud	7	2.3	3.9	3.1	-1.1	99	0.7
10.11.03 0500	10.11.03 1000	in cloud	5	4.0	4.2	3.6	-0.6	99	2.2
30.11.03 0300	30.11.03 0900	in cloud	6	1.6	4.9	3.9	-0.9	98	0.7
4.12.03 2100	5.12.03 0700	in cloud	10	2.0	4.0	3.5	-0.7	98	0.7
28.12.03 0500	28.12.03 2100	in cloud	16	1.8	3.3	3.1	-5.2	92	1.1
29.12.03 2200	30.12.03 0800	in cloud	10	1.6	2.6	3.4	-0.7	98	0.9
30.12.03 1900	31.12.03 0300	in cloud	8	2.1	iced	iced	-5.6	100	1.2
07.01.04 0500	07.01.04 0600	in cloud	2	2.5	3.4	2.6	-8.2	93	0.4
08.01.04 0600	09.01.04 0700	in cloud	14	2.3	2.5	3.2	-2.7	93	1.4
26.01.04 1600	27.01.04 1100	in cloud	35	1.5	3.1	3.1	-5.9	95	1.6
10.01.04 0800	10.01.04 1000	freezing rain	2	4.3	6.0	5.3	0.4	94	0.7
12.01.04 2100	12.01.04 2200	freezing rain	1	4.5	4.2	3.7	0.2	91	0.6
25.01.04 1100	25.01.04 1800	in cloud + freez.rain	1	1.0	3.1	2.5	-4.8	89	0.3

The distribution of accreted icemass in Oberstrahlbach during the two winters 2002/2003 and 2003/2004 is shown in Figure 5.1. As it can be seen severe icing did not occur during the observation period, with 85% of all cases not exceeding 1 kg/m².

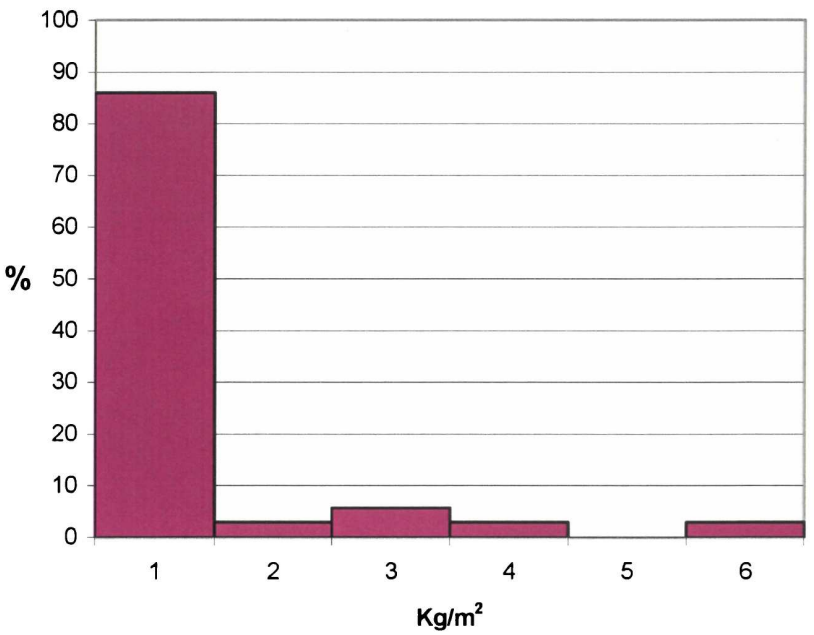

Figure 5.1: Distribution of measured ice mass in Oberstrahlbach, winter 2002/2003 and 2003/2004

The distribution of air temperature during the icing processes is presented in Figure 5.2. The maximum number of the icing cases occurs in Oberstrahlbach in the temperature interval from - 4 to –6°C.

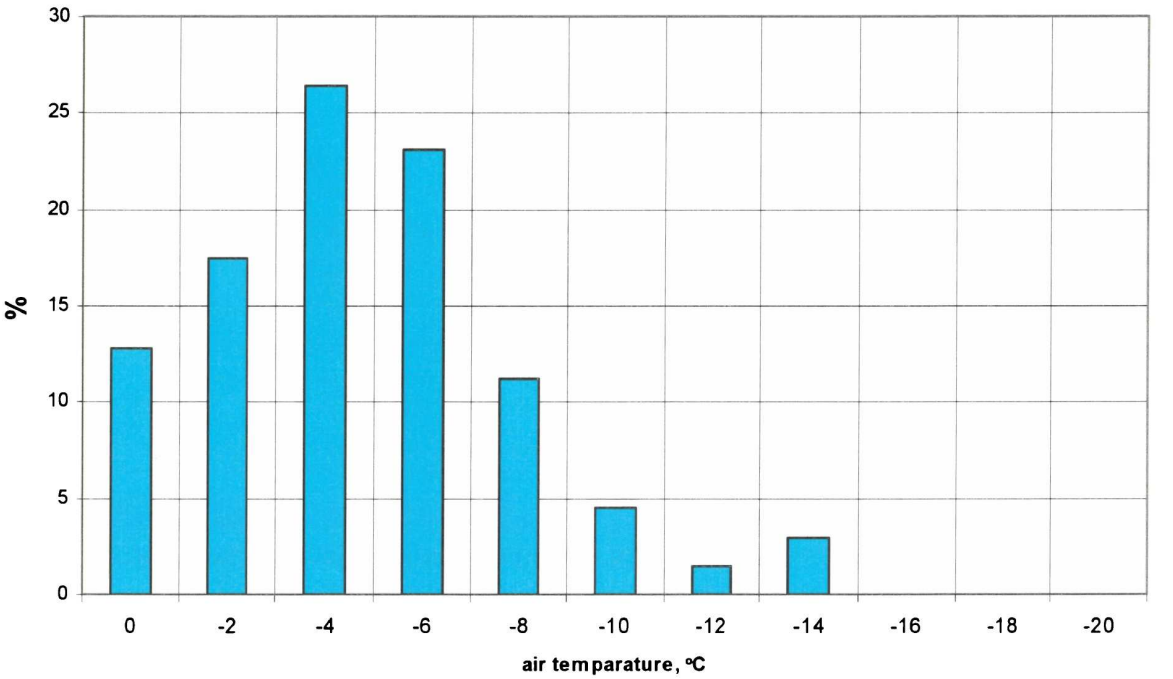

Figure 5.2: Distribution of air temperature during icing phases given in Table 5.1 and 5.2 (Oberstrahlbach)

In Figure 5.3 and Figure 5.4 the distribution of the wind speed for the heated and unheated anemometer at 20 m and 40 m are presented. It can be seen that the icing effects change the frequency distribution significantly, especially for the 40 m data, giving a maximum for lower wind speeds and showing the frequent freezing of the unheated wind sensor.

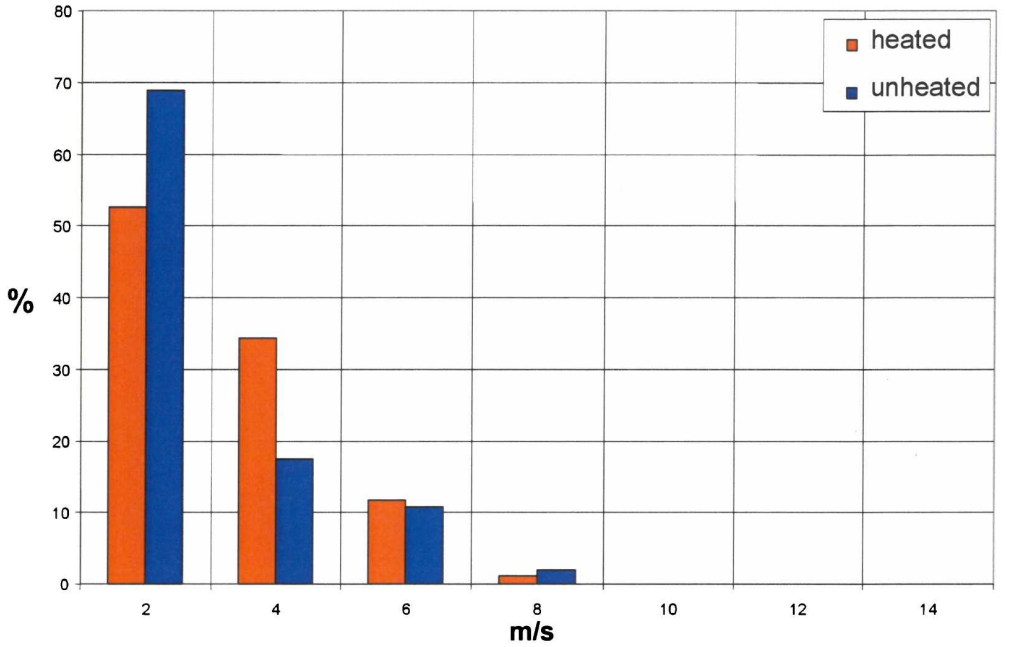

Figure 5.3: Distribution of wind speeds for heated and unheated anemometers at 20 m above ground level during icing phases given in Table 5.1 and 5.2 (Oberstrahlbach)

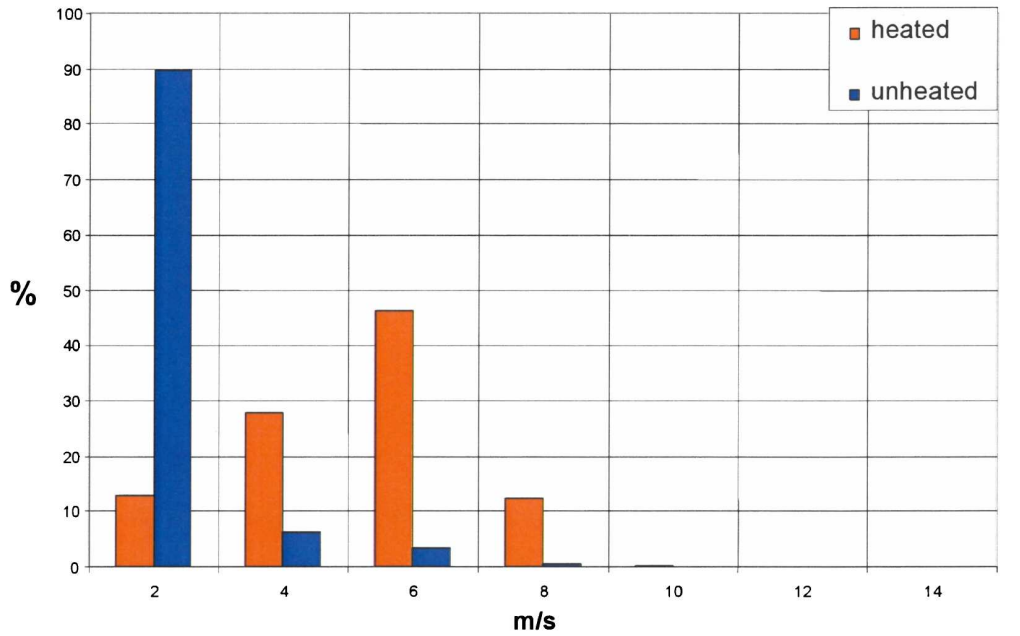

Figure 5.4: Distribution of wind speeds for heated and unheated anemometers at 40 m above ground level during icing phases given in Table 5.1 and 5.2 (Oberstrahlbach)

5.3. Comparison of the experimental data and different icing model results

5.3.1 Freezing rain

From Table 5.1 and 5.2 it can be seen clearly that the icing intensity is greatest during freezing rain. A good correlation between the icing rate and the precipitation rate has been found for the freezing rain cases and is presented for these listed in Tables 5.1 and 5.2 in Figure 5.5 giving an icing intensity $I = 0{,}0036\,P$.

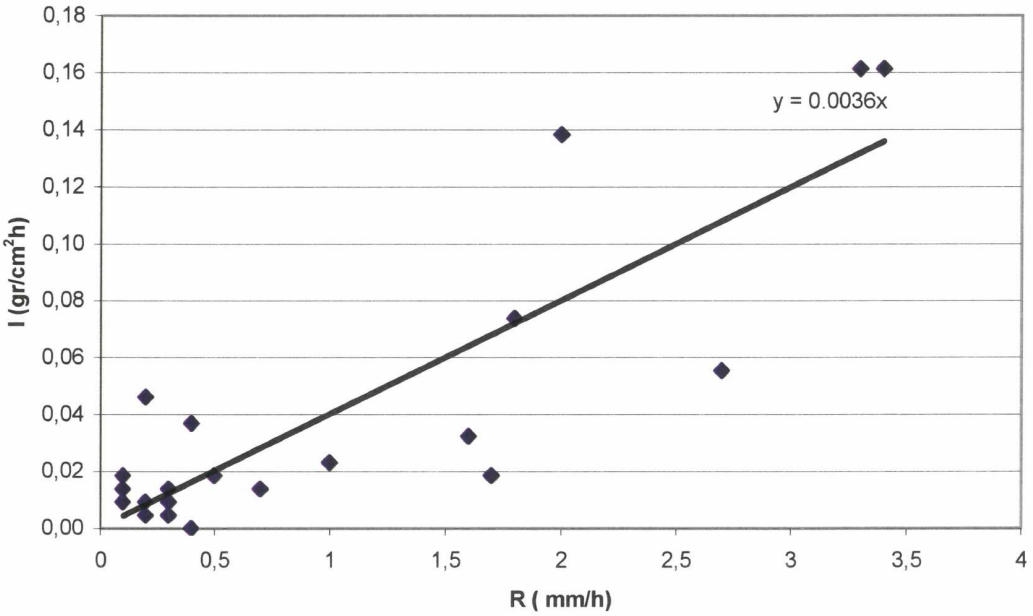

Figure 5.5: Precipitation rate R versus icing intensity I; Oberstrahlbach (see text)

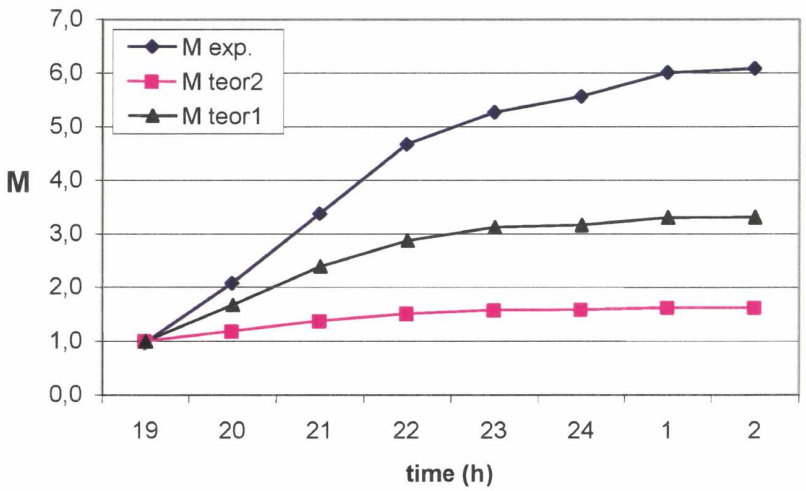

Figure 5.6: Measured M_{exp} and calculated cumulative ice mass M (kg/m²) for freezing rain in the time period 22.-23.12.2002 (Oberstrahlbach); M_{teor1} with Eq.(3.45), M_{teor2} with Eq.(3.47).

For quantifying the relationship between precipitation and icing during freezing rain Eq.(3.45) after Sundin and Makkonen (1998) was used for a first rough estimation, though this formula is valid only for vertical surfaces, assuming that the freezing fraction of the falling water droplets is 1, c.f. that all droplets are freezing. The results are shown in Figure 5.6 for the freezing rain event from 22.12. to 23.12.2002 together with the measured ice mass. As can be seen, the results are much lower than the measured values which may have been caused by the combined influence of in-cloud icing and freezing rain.

5.3.2 In cloud icing

From the measurements in Oberstrahlbach and Sternstein the following findings are presented.

Figure 5.7 shows the measured icing intensity, the wind speed and the calculated intensity from Eq. (4.3a) after Ahti and Makkonen (1982). Due to the broadly scattered data this estimation is considered unsatisfactory.

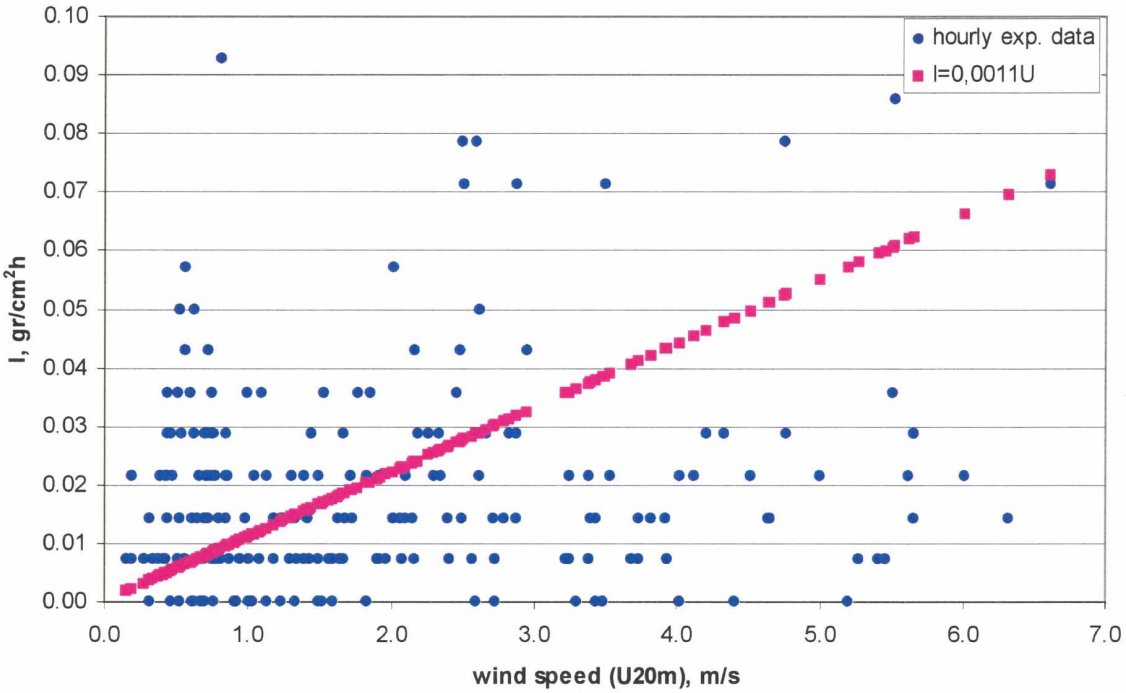

Figure 5.7: Calculated and measured icing intensity I vs. wind speed (Oberstrahlbach)

In the next graph (Figure 5.8) the two approaches after Ahti and Makkonen.(1982, Eq.(4.3a)) and Tammelin et al. (1996, Eq.(4.3c)) are given, showing a remarkable difference in the results. The average icing intensity for each icing event was taken here as a base.

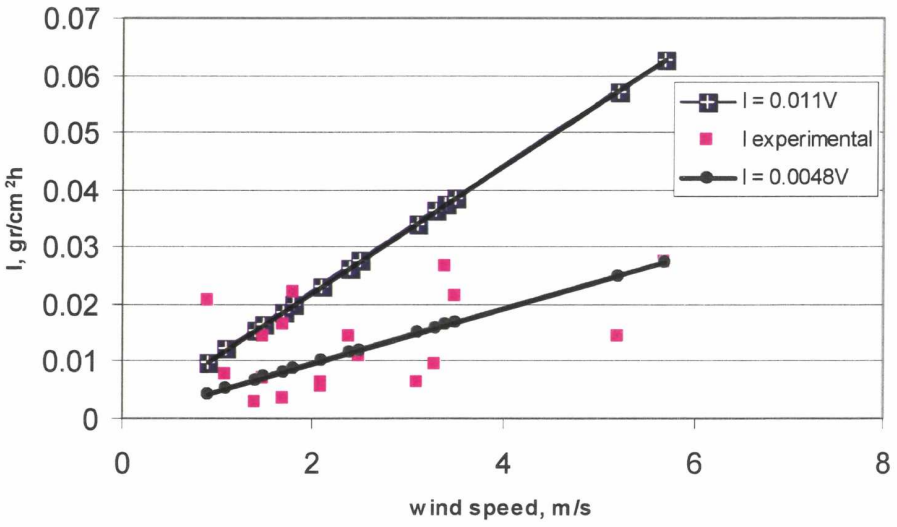

Figure 5.8 Relation between wind speed at 20 m height and average icing intensity I after Eq.(4.3a) and Eq.(4.3c)

However there is a good correlation between ice mass and the duration of the process when multiplied by wind speed, as presented in Figure 5.9. A better correlation is obtained if instead of using the values for the supposedly iced anemometers at 20 m height (blue) the values for 40 m height (pink) are used. This can be taken as an indirect confirmation that the heated anemometer at 20 m is also frequently affected by icing. The derived relationship from Figure 5.9 extrapolated for 10 m height above ground level gives

$$M_{10} = 0{,}039\, t\, V_{10} \tag{5.1}$$

with M the mass of rime ice accretion, t the time of duration of ice accretion in hours and V the wind speed in m/s for an air temperature below 0°C. This is in comparatively good agreement with the height dependent findings of Tammelin et al.(1996)

$$M(z) = a_z\, 0{,}11\, t_z\, V_z \tag{5.2}$$

who included a factor to account for the cloud amount which is set in Eq.(5.1) to unity.

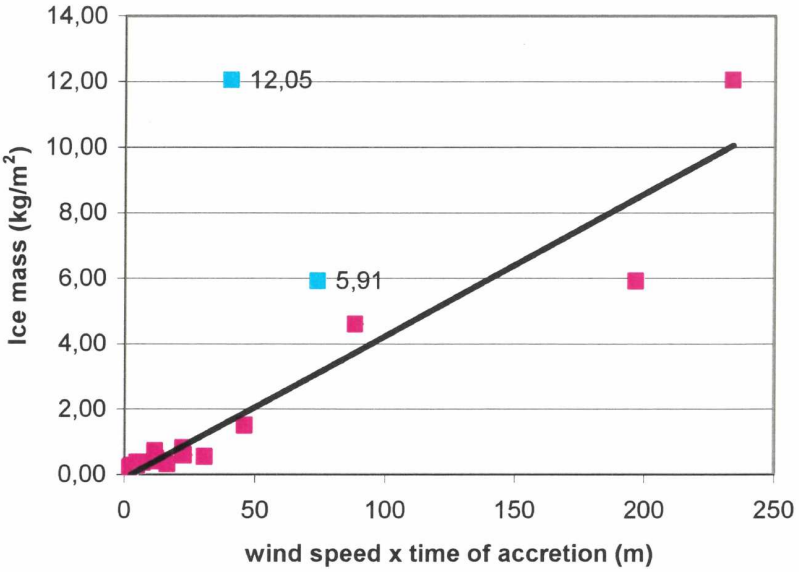

Figure 5.9: Mass of rime ice accretion vs. wind speed in two heights (blue at 20 m, pink at 40 m) and duration of the icing process (averages of each single icing event in Oberstrahlbach)

The icing intensity dependent on wind speed shown in Figure 5.10 reveals only a weak correlation in Oberstrahlbach. The relation $I = 0{,}0044\ V_{20}$ is of the same order of magnitude as the relation after Eqs.(4.3a)-(4.3c).

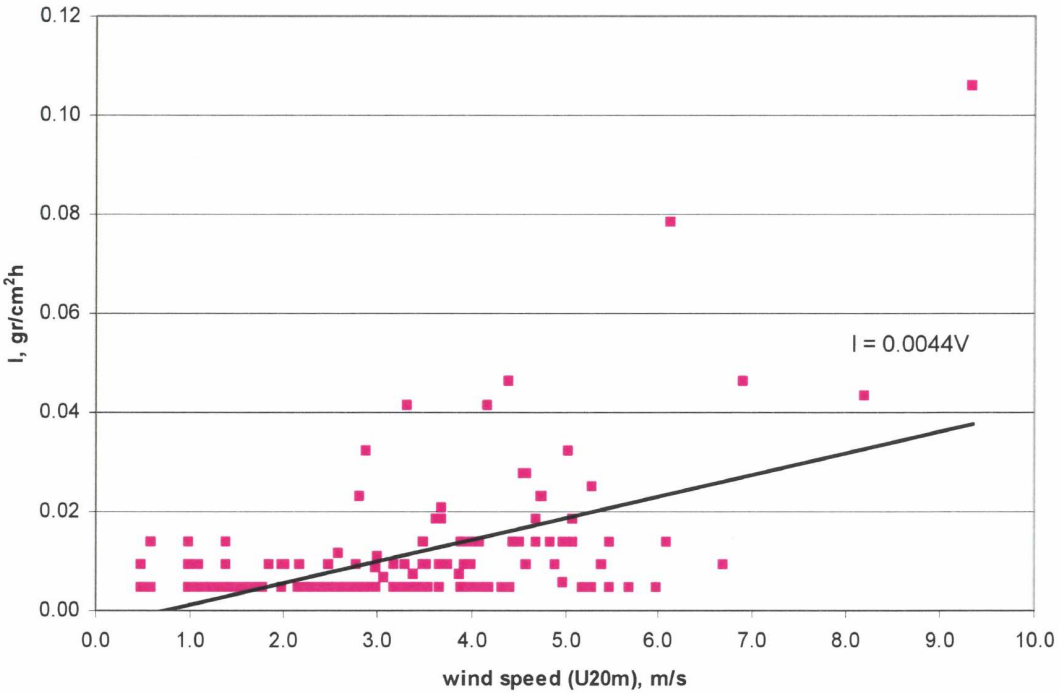

Figure 5.10: Correlation between the wind speed (at 20 meter height) and icing intensity, Oberstahlbach (see text)

Results from the short measuring period in Sternstein from similar measuring equipment as Oberstrahlbach are shown in Figure 5.11. This figure contains all cases with icing giving a little more distinct correlation between wind and icing intensity than shown in Figure 5.10. This is because in Sternstein the icing events were much more severe than in Oberstrahlbach.

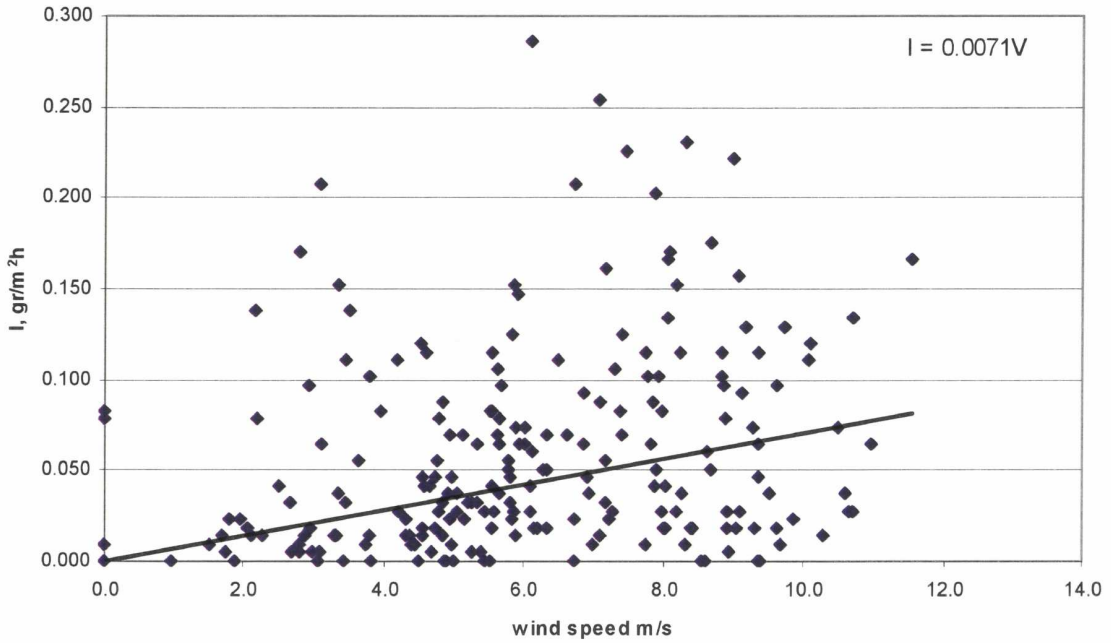

Figure 5.11: Wind speed versus icing intensity I in Sternstein, all cases

The estimation of the ice mass for in-cloud icing (after Ahti and Makkonen 1982) in the form of Eq.(4.3a) was used. As an example of an icing event the case of 20.12.2002 (number 1 in Table 5.1) is given. The experimental and calculated results are presented in Figure 5.12. The data disagree widely and measured data is significantly over estimated. Various reasons for this could result from low liquid water content, small drop size relative to reduced air temperatures or error in wind speed measurement due to anemometer icing.

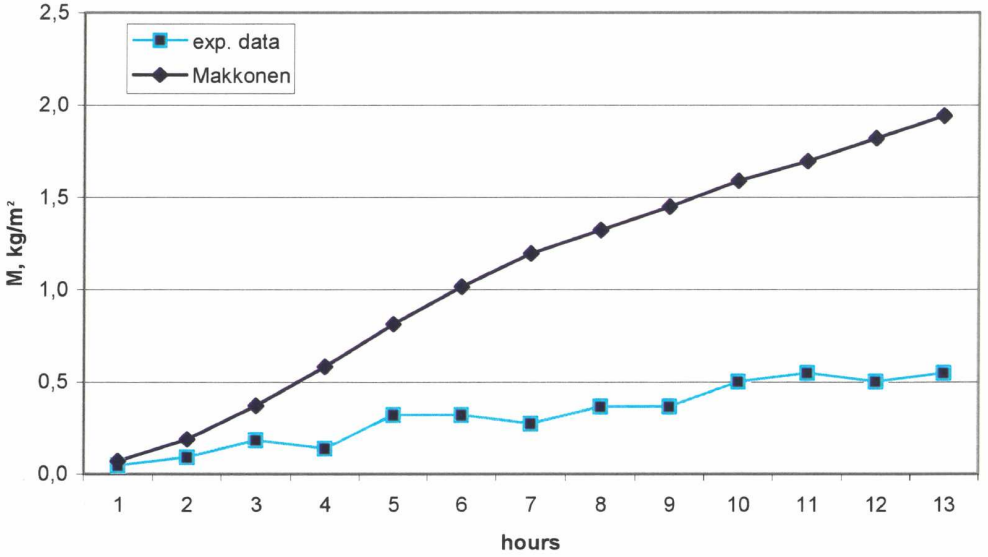

Figure 5.12: Measured and calculated (after Eq.4.3a) ice mass M (kg/m²) for the icing event on 20.12.2002 (Oberstrahlbach)

The next figures (Figure 5.13 and 5.14) show two phases of a long icing event without full melting between the them. In the first phase the calculations show again an overestimation by Eq.(4.3a) compared with the present experimental data. The measured intensity increased gradually at first (Figure 5.13) but after about 17 hours a steeper rise can be observed. An explanation for this behaviour could be that the ice growth is wet at the beginning (lower icing efficiency) and after 17 hours it turns to dry growth with a higher intensity rate.

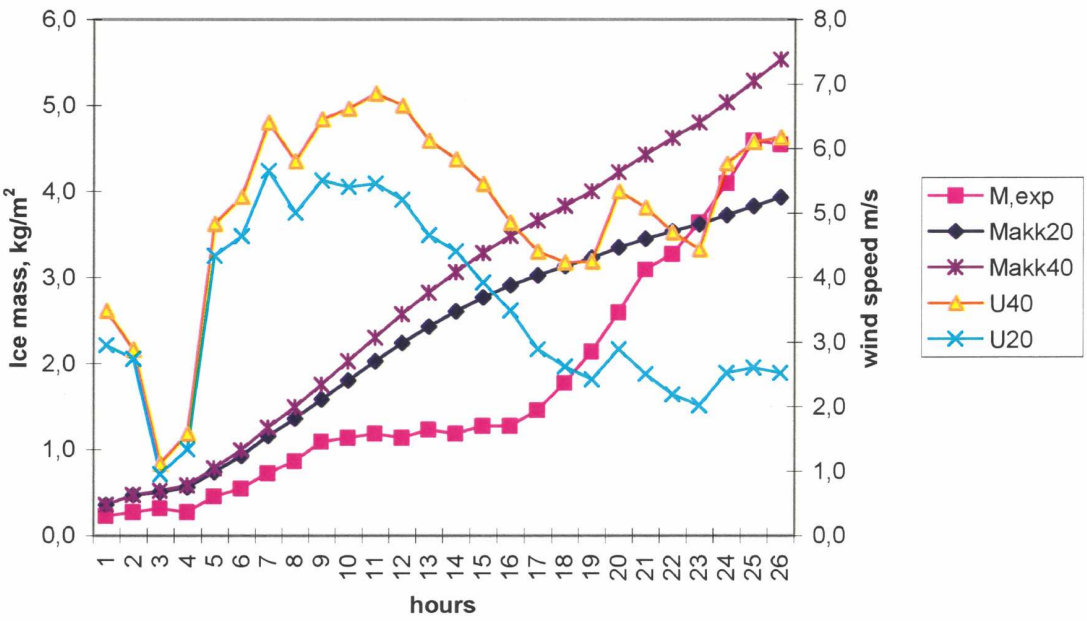

Figure 5.13: Icing period 23.-28.12.2002; first phase (see text)

Figure 5.14 depicts the icing process starting with an ice accretion mass of ca 4 kg/m^2. The process starts without full melting of the previously deposited ice. In the first 20 hours there is a slight overestimation and after that time the model results are significantly different from the measured data, which is related to the lower wind speeds at this time. Probably the wind speed measurements were influenced by icing on the anemometers as shown by the results at 20 m height (U20).

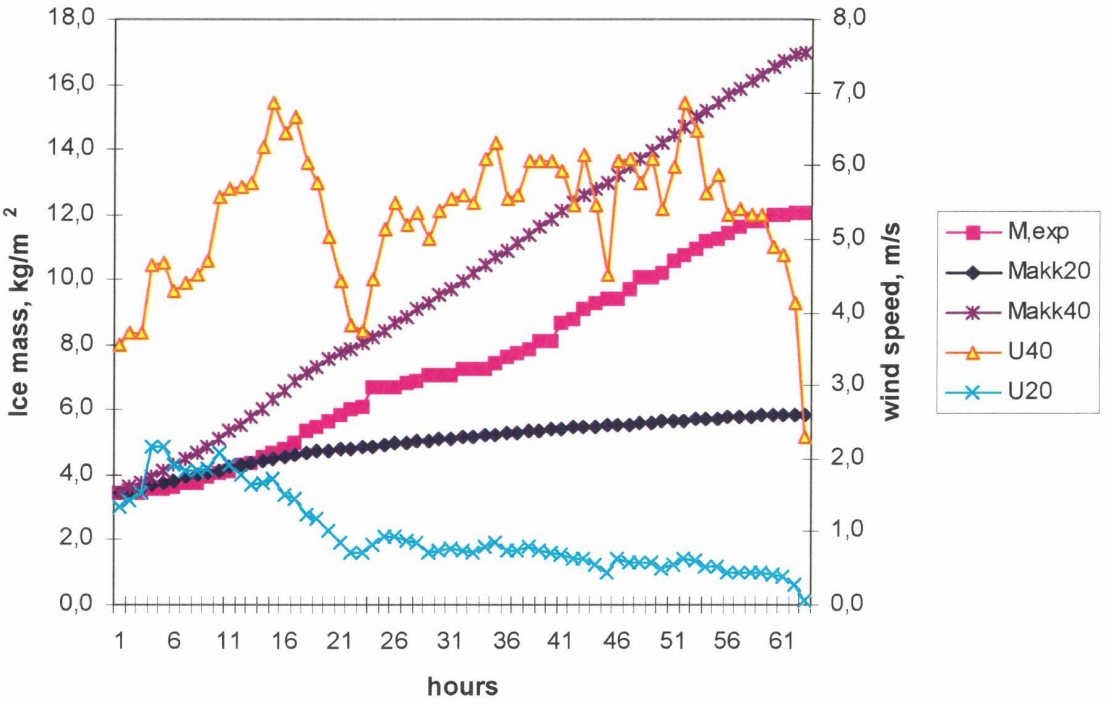

Figure 5.14: Icing period 23.-28.12.2002; second phase (see text)

The following cases shown here are calculated from Eq.(3.14) after Makkonen (1981). The calculation of LWC was made possible using (starting January 2003) pictures from web cameras in relationship with the horizontal visibility (Stanev et al. 1987, Stanev and Moraliiski 1987). In Figure 5.15 the conditions for the case from 20th to the 22nd January 2003 are shown. The first curve, M(teor1), depicts the results for a fixed mean value of LWC = 0.5 gr/m^3. The second curve, M(teor2), calculated with the wind speed at 20 m above ground level using Eq.(3.1a) shows the results of the calculation with hourly values of LWC from the afore mentioned relation after Stanev et al. (1976). This curve is closer to the measured data for the first 12 hours of the process. After that time there is a considerable difference, which is probably due to the higher collection efficiency E (in the calculation E has a constant value). Here it is observed again that the wind speed decreases, which is probably due to icing of the anemometer at 20m height, as previously described in the initial phases of the icing event. As both approaches underestimate the actual ice mass it is strongly evident that a good understanding of the parameters for each time interval and the underlying principles for this application is fundamental.

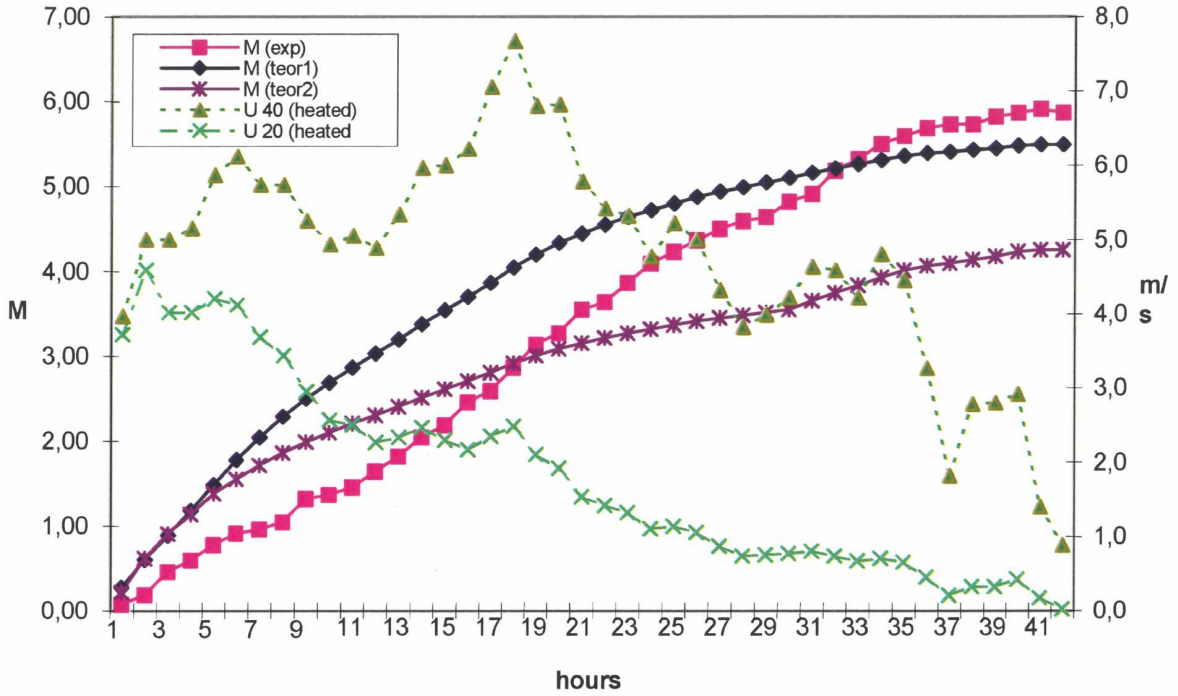

Figure 5.15: Calculated and experimental data for ice mass M (kg/m²) for the event from 20.-22.1.2003. Oberstrahlbach. M(theor2) derived with Eq.(3.1a), M(theor1) derived with a fixed value of LWC = 0.5 gr/m^3

5.4 Icing and energy production

As mentioned above, the test site in Oberstrahlbach has installed a Vestas V44 with 600 KW rated output and 63 m hub height. A comparison of the operating data for this turbine with the meteorological and icing data is given in Figure 5.16 for the winter 2002/2003. Here the orange dots indicate hours with an icing mass of more than 5 g measured by the ice sensor. The blue diamonds indicate hours with no icing. The value of the calculated power output was estimated with the wind at 40 m height. Beside the times of stand still of the turbine one can identify a diminished power output during the hours of icing of about 10 % at comparatively low wind speeds below 300 kW. Most of the stand still time of the turbine during the two winters in Oberstrahlbach was not caused by the icing situation. The ice load was considered not severe enough to stop the wind turbine.

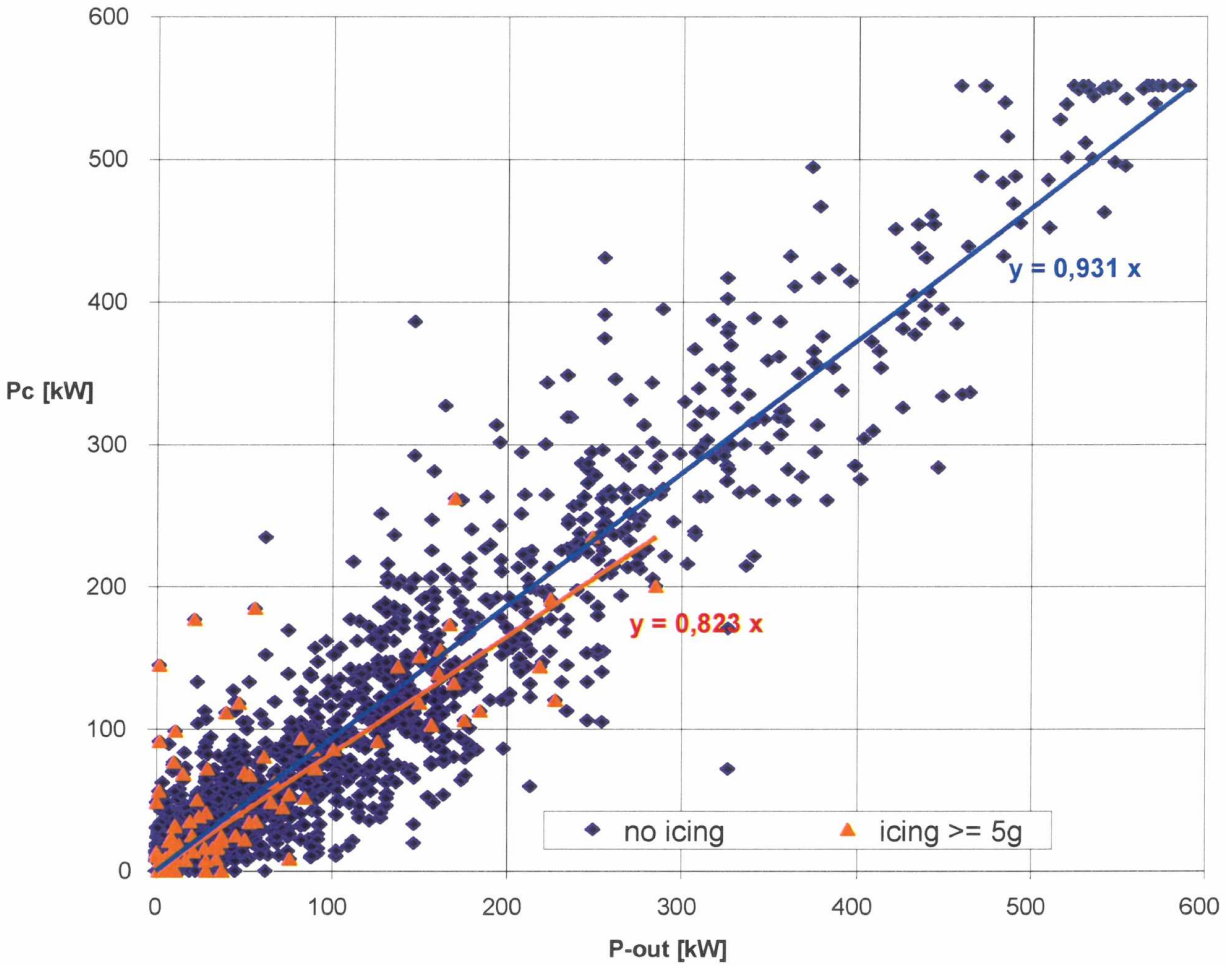

Figure 5.16: Calculated (Pc) and actual power output (P-out) for the VESTAS V44/600, Oberstrahlbach (see text).

The course of an icing event is shown in Figure 5.17 for the time period 22.12.-28.12.2002. At the beginning of this period low wind speeds caused only very little power output with icing increasing quickly in the second half of the first day. After an air mass change the ice melted quickly away, and due to increased speed the power output was high. At the end of the second day when the wind speed was again reduced icing started steadily and the turbine power was shut down accordingly. This situation lasted for about four days and the ice mass reached a peak value of about 250 g. This condition ceased when a passing front caused a sudden melting of the ice mass and power production was commenced immediately. During the stand still period of the turbine the wind speed was relatively high at about 5 m/s.

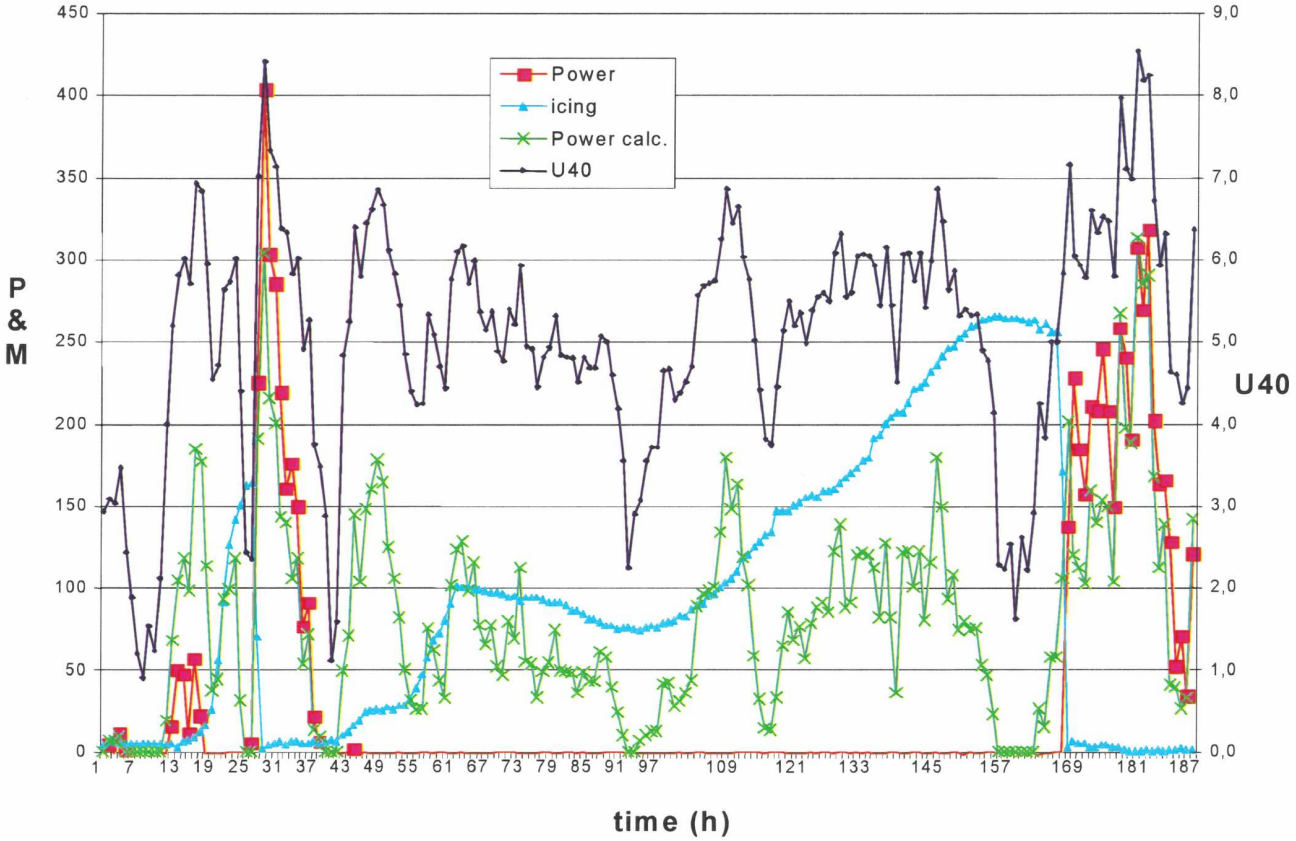

Figure 5.17: The icing event from 22.-29.12.2002; measured and calculated power P (kW) is shown as well as the wind speed at 40 meter (m/s) and the ice mass M (g)

6. Resume

Because the above discussed icing measurements have been gained over relatively short investigation periods it is desirable to compare them with icing conditions at similar sites and with the general icing conditions for central and south Eastern Europe (Table 7.1). This is demonstrated here with data from two meteorological stations situated at comparable altitudes in Bulgaria having long periods of measurements and one at Sternstein, Czech Republic, near the border with Austria (measurements only for the period January to April 2004).

There is a relatively good agreement of the mean characteristics for the icing process, i.e. mean wind speed, mean air temperature and duration. For the sites in Bulgaria the ice load values are for two years and those for Oberstrahlbach and Sternstein are the maximal registered ice masses during the measurement period.

Icing effects are strongly dependent on the location of the measurement. Oberstrahlbach has on average less severe icing events and, therefore, the findings based on the available models are not satisfactory. The height dependency in pre-Alpine areas is shown by the example of Oberstrahlbach and Sternstein (where short period icing measurements were made during winter 2003/2004) which is situated only 20 km West of Oberstrahlbach and lays in the same climatic zone with a 450 meter difference in altitude. As shown, the icing conditions at Sternstein are more severe than at Oberstrahlbach. This is due to the increased elevation, humidity and wind velocity. However, the measurement period in Sternstein was not long enough to provide a statistical significance for these findings.

Table 7.1: Comparison of the mean characteristics for the icing process at different sites in Europe

	Country	Altitude, m	mean wind velocity, m/s	mean air temperature during icing, °C	mean duration of icing hours	max. ice load, kg/m
Oberstrahlbach	Austria	657	3.7	-4.4	10	0.4*
Vakarel	Bulgaria	851	4.2	-3.8	12	2.2**
Sternstein	Czech Republic	1122	6.1	-5.1	28	2.9*
Petrohan	Bulgaria	1400	4.0	-5.8	24	6.0**

* observed in the period of investigation, ** average for the last two years

From the results discussed in paragraph 5.3 it can be reasoned that they are partly unsuitable because of

- variation in the liquid water content
- variation in the drop size
- the existence of wet growth processes,
- icing of the heated anemometer,
- the Trabert formula for assessing LWC in the form of Eq.(3.1) was originally derived for daily mean values; not using hourly values may be not appropriate in this case.

The examples presented here show in general good agreement for freezing rain but for the other types of icing more accurate results are necessary. To gain this improved information about the liquid water content and the droplet size spectrum has to be provided. From another measurement site with only a measurement period of about two month (Sternstein measurements) the correlation between the wind velocity and icing intensity is clearer and more intense icing happened at this location.

7. References

Aufm Kampe, H. J., H. K. Weickmann (1952): Trabert's formula and the determination of water content in clouds. *J. Meteor.*, 9, 17-85.

Aufm Kampe, H. J, H. K. Weickmann, J.J.Kelly (1956): A continuously measuring water content meter. *J. Meteor.*, 13, p.64.

Admirat, P., Y. Sakamoto (1988): Wet snow on overhead lines: state of art. *In Proc. 4th Int. Workshop on Atmospheric Icing of Structures*, pp. 8-13.

Ahti, K., L. Makkonen (1982): Observation on rime formation in relation to routinely measured meteorological parameters. *Geophysica* 19, 75 85

Baranowski, S., J. Liebensbach (1977): The intensity of different kinds of rime on the upper tree line in the Sudety mountains. *J. Glaciol.* 19, 489-497.

Best, A. C. (1950): The size distribution of raindrops. *Quart. J. Roy. Meteor. Soc.* 76, 16-36.

Best, A. C. (1951): Drop size distribution in cloud and fog. *Quart. J. Roy. Meteor. Soc.* 77, 418-428.

Blackmore, R. Z., L. Makkonen, E. P. Lozowski (2002): A new model of spongy icing from first principles. *J. Geophys. Res.* 107, D21, 13 p.

Buchinski, V. E. (1969): *Icing and its prevention.* Leningrad, *Gidrometeoizdat.*

Cansdal, J. T., R. W. Gent (1983): Ice accretion in two-dimensional compressible flow – a theoretical model. RAE Technical Report 82128

Chaine, P. M., P. Skeates (1974): Wind and ice loading criteria selection. Canadian Climate Central Internal Report, Industrial Meteorology – Study III, Atmospheric Environment Service, Ontario, Canada.

Clift R., J.R.Grace, M.E.Weber (1978): Bubbles, Drops and Particles. Academic Press, London

Cornford, S. G. (1965): Fall speeds of precipitation elements. *Quart. J. Roy. Meteor. Soc.*, 91, 91-94.

Diem, M. (1942): Messungen der Größe von Wolkenelementen I, *Ann.d.Hydrogr.* 70, p.142.

Diem, M. (1948): Messungen der Größe von Wolkenelementen II, *Met. Rundschau* 1, p. 261.

Dranevic, E. P. (1971): Glaze and rime. Leningrad, *Gidrometeorologitschesko* (in Russian).

Dufor, L. (1861): Arch. Sci. Phys. et Nat., 10, p.346.

Finstad, K. J., E. P. Lozowski, L. Makkonen (1988a): On the median volume diameter approximation for droplet collision efficiency. *J. Atmos. Sci.* 45, 4008-4012.

Finstad, K. J., E. P. Lozowski, E. M. Gates (1988b): A computational investigation of water droplet trajectories. *J. Atmos. Oceanic Tecjnol.* 5, 160-170.

Gluchov, V. G. (1989): *Tall building icing on plain territory of the USSR.* Leningrad, *Gidrometeoizdat* (in Russian).

Goodwin III, E., J., J. D. Mozer, A. M. DiGioia Jr., B. A. Power (1983): Predicting ice and snow loads on transmission lines. Proc. First International Workshop on Atmospheric Icing of Structures, 267-273.

Holodov, V. U., N. I. Popov (1976): The effect of structural parameters of electric overhead lines on iceloads on cables. *Trudy* GGO 379, 30-36 (in Russian).

ISO 12494 (2000): Atmospheric Icing of Structures. ISO/TC 98/SC3.

Jones, K. F. (1990): The density of natural ice accretions related to non-dimensional icing parameters. *Quart. J. Roy. Meteor. Soc.* 119, 599-604.

Jones, K. F. (1996): Ice accretion in freezing rain. *US Army Cold Regions Research and Engineering Laboratory Report*, 1-22.

Knight, C. A. (1968): On the mechanism of spongy hailstone growth. *J. Atmos. Sci.* 25, 440-444.

Langmuir, I., K. B. Blodgett (1946): A mathematical investigation of water droplet trajectories. In *Collected works of Irving Langmuir*, vol. 10, pp. 335-393. Oxford, Pergamon press.

Levi, L., O. B. Nasello, F. Prodi (1991): Morphology and density of ice accreted on cylindrical collectors at low values of impaction parameter; I: Fixed deposits. *Quart. J. Roy. Meteor. Soc.* 117, 761-782.

List, R. (1977): Ice accretion on structures. *J. Glaciol.* 19, 451-465.

Lomilina, L. E. (1977): The effect of relief on glaze-ice and rime deposition. *Sov. Meteor. Hydrol.*, 2, 39-43.

Lozowski, E. P., (1978): Stochastic effects in spray droplet sampling with oiled slides. Lab. Memo. LT-172. Low Temperature Laboratory, Division of Mechanical Engineering, National Research Council of Canada, Ottawa, Canada.

Lozowski, E. P., J. R. Stallabrass, P. F. Hearty (1983): The icing on unheated, nonrotating cylinder. Part I: A simulation model. *J. Climate Appl. Meteor.* 22, 2053-2062.

Lozowski, E. P., J. R. Stallabrass, P. F. Hearty (1983): The icing on unheated, nonrotating cylinder. Part II: Icing wind tunnel experiments. *J. Climate Appl. Meteor.* 22, 2063-2074.

Ludlam, F. H. (1950): The composition of coagulation elements in cumulonimbus. *Quart. J. Roy. Meteor. Soc.*, 76, p. 52.

Ludlam, F. H. (1951): The heat economy of a rimed cylinder. *Ouart. J. Roy. Meteor. Soc.*, 77, 663-666.

Ludlam, F. H. (1958): The hail problem. Nubila, 1, p.13.

McKay, G. A., H. A. Thompson (1969): Estimating the hazard of ice accretion in Canada from climatological data. *J. Appl. Meteor.* 8, 927-935.

Macklin, W. C. (1962): The density and structures of ice formed by accretion. *Quart. J. Roy. Meteor. Soc.* 88, 413-424.

Macklin, W. C., G. S. Payne (1968): Some aspects of the accretion process. *Quart. J. Roy. Meteor. Soc.* 94, 167-175.

Maeno, N., T. Takahashi (1984): Studies on icicles. I. General aspects of the structure and growth of an icicle. Low Temp. Sci. A 43, 125-138 (in Japanese).

Maeno, N., L. Makkonen, K. Nishimura, K. Kosugi, T. Takahashi (1994): Growth rate of icicles. *J. Glaciol.* 40, 319-326.

Makkonen, L. (1981): Estimating intensity of atmospheric ice accretion on stationary structures. *J. Appl. Metor.* 20, 595-600.

Makkonen, L. (1984): Modelling of ice accretion on wires. *J. Climate Appl. Meteor.* 23, 929-939.

Makkonen, L. (1985): Heat transfer and icing on a rough cylinder. *Cold Regions Science and Technology* 10, 105.

Makkonen, L., J. R. Stallabrass (1987): Experiments on cloud droplet collision efficiency of cylinder. *J. Climate Appl. Metor.* 26, 1406-1411.

Makkonen, L. (1988): A model of icicle growth. *J. Glaciol.* 34, 64-70.

Makkonen, L. (1989): Estimation of wet snow accretion on structures. *Cold Regions Sci. Technol.* 17, 83-88.

Makkonen, L., Y. Fujii (1993): Spacing of icicles. *Cold Regions Sci. Technol.* 21, 317-322.

Makkonen, L., K. Ahti (1995): Climatic mapping of ice loads based on airport weather observations. *Atmos. Res.* 36, 185-193.

Makkonen, L. (1998): Modelling power line icing in freezing precipitation. *Atmos. Res.* 46, 131-142.

Makkonen L. (2000): Models for the growth of rime, glaze, icicles and wet snow deposits on structures. Philosophical Transaction A, vol. 358, pp. 2913-2939.

Makkonen, L., T. Laakso, M. Marjaniemi, K. J. Finstad (2001): Modelling and prevention of ice accretion on wind turbines. *Wind Engineering*, 25, 3-21.

Mason, B. J. (1957): The physics of clouds. Oxford, Clarendon Press.

Matveev, L. T. (1984): Course of general meteorology. Atmospheric Physics. Leningrad. *Gidrometeoizdat* (in Russian).

Mazin, I. P. (1957): Physical principles of aircraft icing. Leningrad: *Gidrometeoizdat* (in Russian).

McComber, P. (1990) Effects of cable twisting on atmospheric ice shedding. Proc. 5th Int. Workshop on Atmospheric Icing on Structures, paper A2-8.

Melcher, D. (1951): Experimental investigations on icing events. *Z. Math. Phys.*, 2, p. 421.

Messinger, B. L. (1953): Equilibrium temperature of an unheated icing surface as a function of air speed. *J. Aeronaut. Sci.*, 20, 29-42.

Michael, D. H. (1968): The steady motion of a sphere in dusty gas. *J Fluid Mech.* 31, 175-192.

Michael, D. H, P. W. Norey (1969): Particle collision efficiency for a sphere. *J Fluid Mech.* 37, 565-575.

Morsi, S. A., A. J. Alexander (1971): Collision efficiency of a particle with a sphere and cylinder. Int. Conf. on the Pneumatic Transport of Solids in Pipes, Paper B2, Cambridge, U.K.

Poots, G. (1996): Ice and snow accretion on structures. Taunton, Research Studies Press.

Prodi, F., L. Levi, P. Pederzoli (1986): The density of accreted ice. *Quart. J. Roy. Meteor. Soc.* 112, 1081-1090.

Prodi, F., L. Levi, V. Levisanni (1986): Ice accretion on fixed cylinder. *Quart. J. Roy. Meteor. Soc.* 112, 1091-1109.

Saffman, P. G. (1962): On the stability of laminar flow of a dusty gas. *J. Fluid Mech.* 13, 120-128.

Schumann, T. E. W. (1938): *Quart. J. Roy. Meteor. Soc.*, 64, p. 3.

Skelton., P. L. I., G. Poots (1991): Snow accretion on overhead line conductors of finite torsional stiffness. *Cold Regions Science and Technology* 19, 301-316.

Souster, G. G. (1979): Technical Report. Department of Building Science, University of Sheffield, U.K.

Stanev, S. E. Moraliiski, K. Velchev (1970): On the rim icing in mountain regions. Hydrology and Meteorology, XIX,Vol.6,pp.15-22 (in Burlgarian).

Stanev, S., E. Moraliiski (1987): Icing of power lines in mountain region. BLMH, vol. 2, 41-44.

Stanev, S., E. Moraliiski, K. Velchev (1987): On the size of supercooled water fog droplet in mountain. *Z. Metorol.* 37, vol. 1, 39-41 (in German).

Sudin, E., L. Makkonen (1998): Ice loads on a lattice tower estimated by weather station data. *J. Appl. Meteor.* 37, 523-529.

Tammelin, B., K. Säntti (1996): Estimation of rime accretion at high altitudes – preliminary results., Proc. of BOREAS III meeting, Finish Meteorological Institute.

Taylor, G.I. (1940): Notes on possible equipment and technique for experiments of aircraft. Aeronaut.Res.Comm.Rep.No.4350.

Wakahama, G., D. Kuroiwa, D. Goto (1977): Snow accretion on electric wires and its prevention. *J. Glaciol.* 19, 479-487.

Weikmann, H. (1953); Precipitation in cumulonimbus. Thunderstorm electricity, Univ. Chicago Press. p. 66.

ANNEX

A. Icing climatology of Europe

A compilation of the relevant data set from WMO RA VI region were applied using some simple models for in cloud icing

A.1 Meteorological data archives

To design an icing potential map the synoptic data for the European domain $\lambda = 10°$ W to 30° E and $\varphi = 35°$ to 75° N and the four Russian stations with WMO-Ids 22028, 22106, 22113, 22127 were collected for the month January to April and October to December in the years 1999-2002. In this domain and time interval 2161 stations were registered; of which 1629 stations were available; 1256 stations provided useful data, of these 75 stations included observations of cloud amount and height of low level clouds and 1000 stations included observations of cloud amount, height and type of clouds. The stated time period was chosen as European synoptic data before the year 1999 are not readily available from archives. These data are stored on tapes with only indirect access, so each set had to be extracted separately for each station in the European domain, requiring nearly 2 hours for each station beside the necessity of large computer resources. Furthermore from 1999 to 2002 a larger number of stations with useful data is available than in the time period 1991 to 1996 (the "WECO" period, Tammelin et al.1998; Tammelin et al.2000) due to the increased number of automatic stations available throughout Europe.

A.2 Collected weather elements from archives:

Synoptic data:

General elements:	- air temperature - dew point temperature - reduced pressure - pressure at station level - visibility - weather code at observation time - weather conditions of last 6 hours - relative humidity - sunshine duration
Precipitation, snow, ice:	- precipitation - snow covered area - total snow depth - fresh fallen snow depth - ice depth
Wind:	- wind direction - wind velocity - wind gust of last 10 minutes

Clouds:
- total cloud amount
- altitude of low level clouds
- cloud amount of low and medium level clouds
- type of low level clouds
- type of medium level clouds
- type of high level clouds
- cloud amount at the 4 lowest levels
- type of clouds of the 4 lowest levels
- altitude of clouds of the 4 lowest levels
- cloud amount below station level
- type of clouds below station level
- upper level of clouds below station level
- appearance of upper level of clouds below station level

Climate data:

- cloud amount
- visibility
- relative humidity

Data of soundings:

At Surface:
- altitude of pressure levels for 1000, 925, 850,700 and 500 hPa:

at Pressure levels
- 1000, 925, 850,700, 500 hPa and surface:
- air temperature
- dewpoint temperature
- wind direction
- wind velocity

significant points:
- pressure
- wind direction
- wind velocity
- air temperature
- dewpoint temperature

A.3 On-site measurements at Oberstrahlbach

Additional meteorological and icing data have been collected at the above described site near Oberstrahlbach, Austria, where the following hourly meteorological data were measured at a 40 m meteorological mast with 3 levels:

- Wind speed and direction (m/s and Deg) at 40 m a.g.l., 10 min. averages
  - Heated: Thies Ultrasonic 2D
  - Unheated: Kroneis 260 PL/P
- Wind speed (m/s) at 20 m a.g.l., 10 min. averages
  - Heated: Kroneis 260 PRH
  - Unheated: Kroneis 260 PL/P
- Temperature (°C) I at 2 m a.g.l., 10 min. averages
- Humidity (%) at 2 m a.g.l., 10 min. averages
- Global radiation (W/m^2) at 2 m a.g.l., 10 min. averages
- Pressure (hPa) at 2 m a.g.l., 10 min. averages

- Data acquisition: Starlog 6004C
- Icing sensor hourly at 3 m
- Pictures from 2 webcams, one pointing to the met mast and the icing sensor the other to the rotor blades of the wind turbine, every 20 minutes

For a rough assessment of visibility wooden white painted poles were driven into the ground at 50 m distance from each other up to a distance of 300 m from the met mast within the view of one of the web cams. This arrangement was used for a rough estimation of the LWC by Eq.(3.1a).

Data about the precipitation rate were taken from the nearby weather station Zwettl (505 m a.s.l.) of the Austrian meteorological measuring network. The icing sensor, provided by the Czech Institute of Atmospheric Research, Prague, was exposed vertically at 3 m height being 461 mm in length and 30 mm in diameter and provided hourly data for the accreted ice mass. Near this measuring site a wind turbine exists, namely a VESTAS V44/600 from which the production data were also gathered hourly.

A.4 Data sets

A.4.1 "Complete" data set

From the domain described in section A.1 484 stations with complete data from January 1999 to March 2002 and observations of wind speed (*V*), temperature (*T*), cloud height (*CH*) and visibility (*Vis*) during day and night were available. For these the number of hours were counted, matching conditions 1–3 (Table A.1), days with at least one observation were counted as one icing day. If the daily observations were made at 3 hourly intervals, the number of intervals were multiplied by 3 to obtain hourly values.

A.4.2 "Incomplete" data set

For the 351 stations in the domain, which have data from January 1999 to March 2002 or observations of *CH* and *Vis* only during daylight, the number of days with at least one observation showing the conditions described in the next section were counted as one icing day. All remaining data have gaps of days or months in the records, or *CH* and *Vis* data are missing for longer time periods and were not considered here.

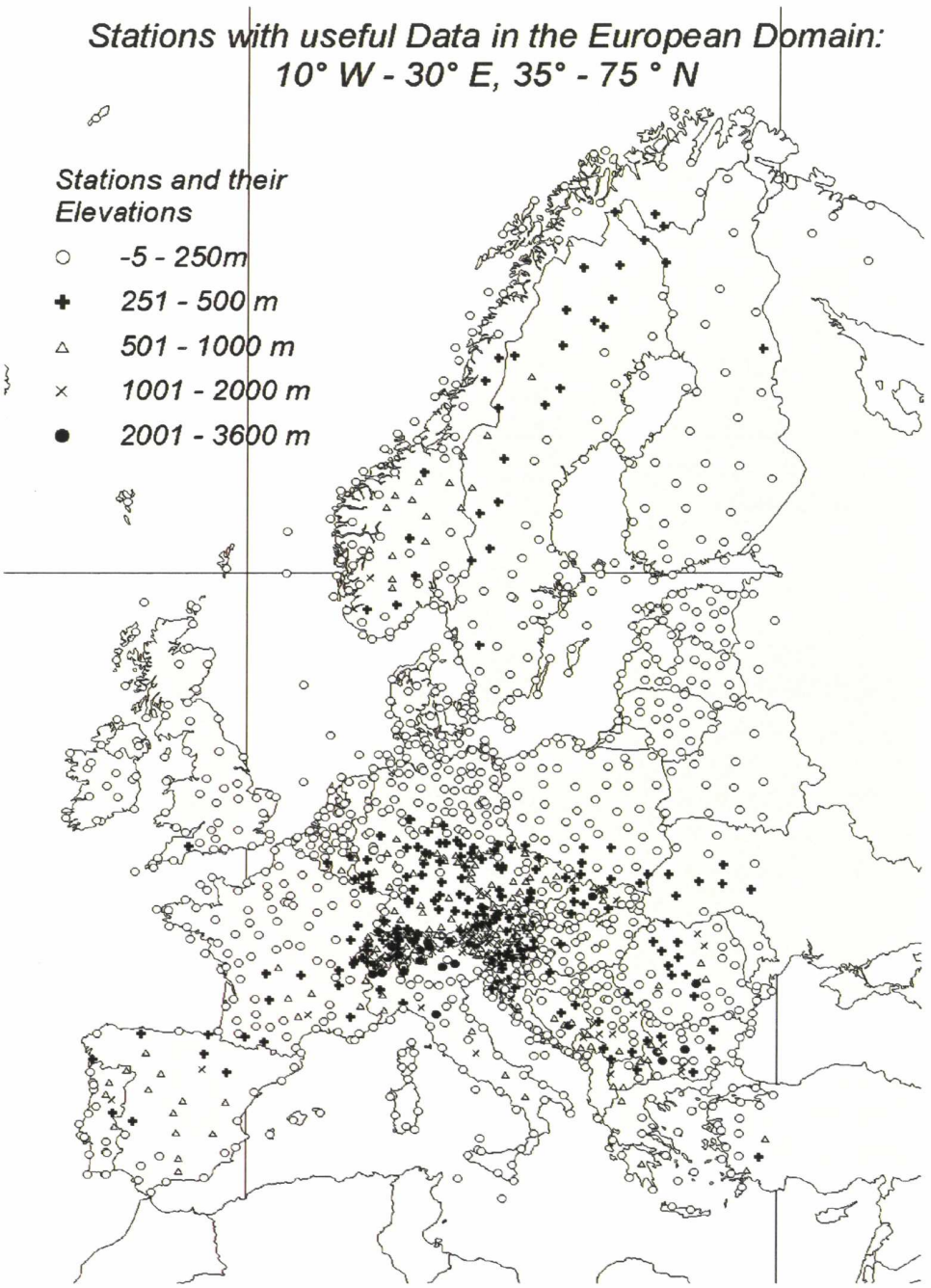

Figure A.1: Station network for which the used data set were derived

A.5 Methods

In order to derive the icing potentials in Europe on the basis of the term icing days (*IcD,* meaning the number of days in the year when icing may occur) the following conditions were examined from the given meteorological data, enhancing such the European Icing Map 1991 – 1996 given in WECO (Tammelin et al.2000). The in-cloud icing conditions used in WECO (method 1 in Table A.1) can only be applied at mountainous sites or high latitudes. Therefore for lower

altitude sites data with visibilities below a certain threshold are chosen for the count of hours with icing events.

Table A.1: Used icing models (T=Temperature, CH=Cloud height, Vis=Visibility; height in m above ground level, V>2m/s)

Model no.	Elements and criteria	Name
1	T in 200 m < 0°C; CH < 200 m	WECO
2	T in 200 m < 0°C; CH < 200 m OR Vis < 1000 m	WECO + Vis
3	T in 200 m < 0°C; CH < 200 m OR Vis < 300 m	WECO + Vis300

Horizontal visibility was added due to the fact that frequently no cloud height was observed as fog was present or there were no cloud observations taken. To better specify these conditions visibility was considered but only when below 300 meters. Visibility alone as defined in meteorology (for fog *Vis* < 1000 meters, Model 2) was not used in this context. In the following analysis and results model 3 is used.

A.6 Results

On the basis of the above described data set and application of the models maps have been designed with ArcView GIS. In Figure A.2 the number of icing days for 100 m above ground level derived after model 3 are mapped, calculating a spatial grid as by Kriging using a spherical variogram model with a lag distance of 5 km, a search radius of 50 km and a grid resolution for the resulting map of 10 km.

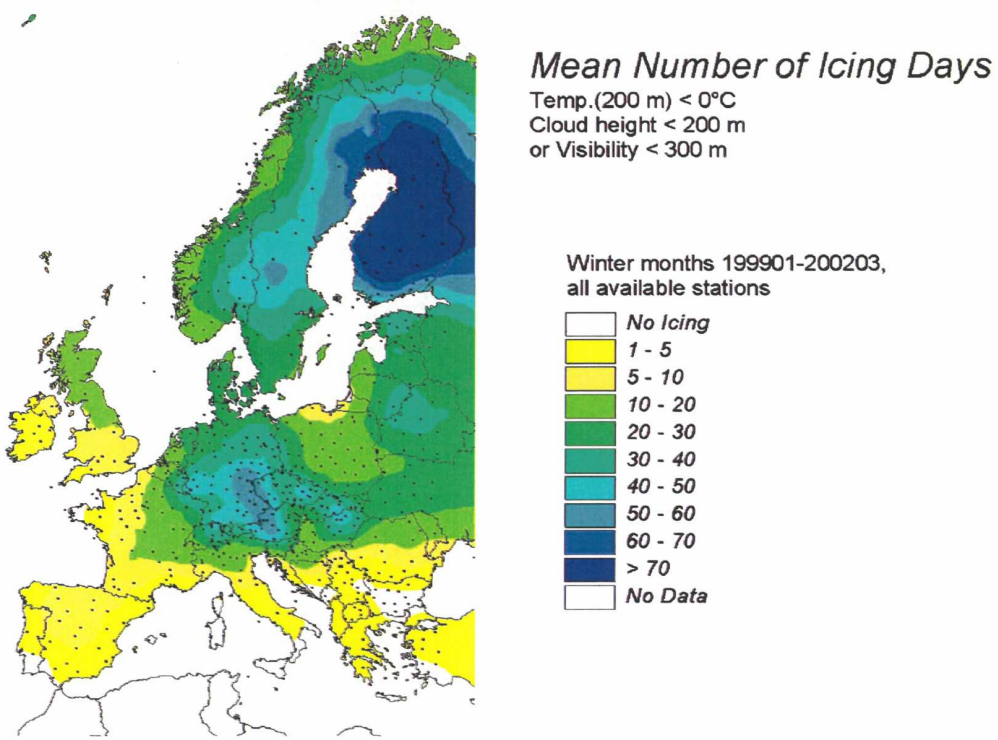

Figure A.2: Mean number of icing days after model 3 at 100 m above ground level.

The expected main features of the large-scale icing distribution are easily recognized. Whereas this model fits quite well in Finland, southern Sweden and Denmark and in the Baltic region (here only at the inland stations) it shows higher deviations along the Norwegian mountain ridge and sea shores when compared to the measured data sets and the findings from WECO (Tammelin et al.2000). Here the *IcD* seems to be underestimated as for the Alps, the Carpathian and Transylvanian mountains.

An improvement of this geostatistical approach and for a more realistic mapping of *IcD* the relationship between longitude (λ), latitude (φ) and height above sea level (H) with the icing events can be used. This is based on the GTOPO30 (30 arc-seconds elevation) global model (U.S. Geological Survey, EROS Data Center). As an example of this kind of approach and the possible functional relationships concerning "*icing climatology*" and its geographic distribution some results are given using a multiple regression model of the form

$$IcD = f(\varphi, \lambda, H, \varepsilon) \qquad \text{(A.1)}$$

in Figure A.3 for northern Europe with a resolution of 0.1 to 0.1 degree. Here ε is a correction function derived by minimising the residuals calculated from the observed and estimated value.

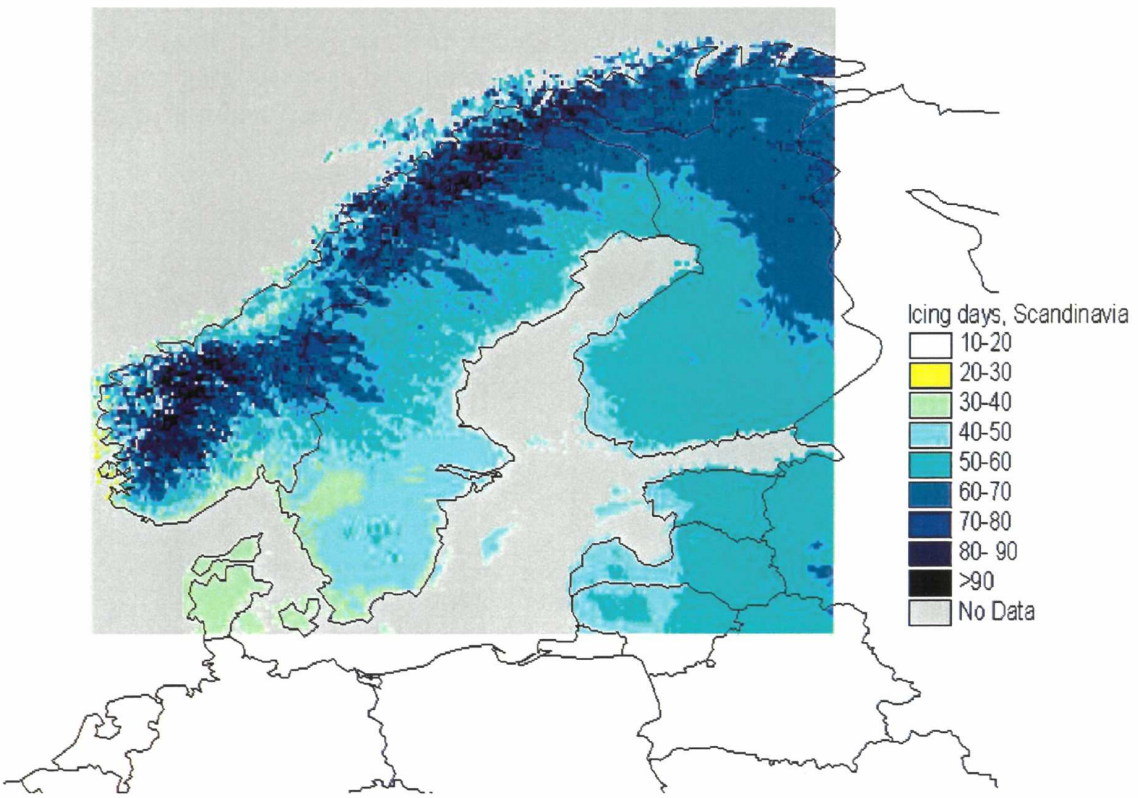

Figure A.3: Icing days calculated with model 3 and Eq.(A.1) for Scandinavia

In the next Figure A.4 a similar approach was used for the Eastern and Northern Alpine region. For statistical reasons the whole alpine area could not to be mapped consistently because in the

Western Alps there seems to prevail different icing conditions due to the influence of the marine climate.

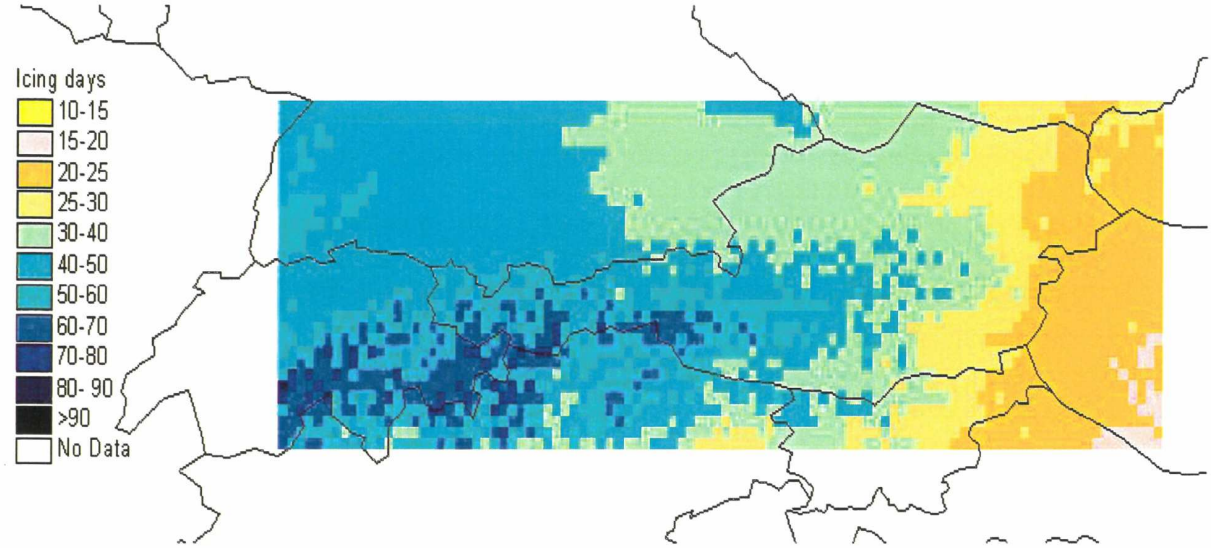

Figure A.4: Icing days calculated using model 3 and Eq.(A.1) for the Eastern and Northern Alpine region

A.7 References

Tammelin B., K. Säntti (1998): Icing in Europe; Proc. BOREAS IV, p.125-132, Finnish Meteorological Institute.

Tammelin B., M. Cavaliere, H. Holttinen, C. Morgan, H. Seifert and K. Säntti (2000): Wind Energy Production in Cold Climate; Meteorolog.Publ.No.41, Finnish Meteorological Institute.

List of Tables

List of Figures

Österreichische Beiträge zu Meteorologie und Geophysik

bisher erschienen:

Heft	Publ.Nr.	Fachgebiet	Autor	Titel und Umfang	Preis in Euro
1	329	Meteorologie		*Tagungsbericht EURASAP, Wien, 14.-16. Nov. 1988, Evaluation of Atmospheric Dispersion Models Applied to the Release from Chernobyl.* Wien 1989, 20 Beiträge, 198 S., 100 Abb., 17 Tab.	14,53
2	332	Geophysik		*Tagungsbericht über das 5. Internationale Alpengravimetrie Kolloquium - Graz 1989.* Herausgeber: H. LICHTENEGGER, P. STEINHAUSER und H. SÜNKEL, Wien 1989, 256 S., 100 Abb., 17 Tab.	vergriffen
3	336	Geophysik		*Schwerpunktprojekt S47-GEO: Präalpidische Kruste in Österreich, Erster Bericht.* Herausgeber: V. HÖCK und P. STEINHAUSER, Wien 1990, 15 Beiträge, 257 S., 104 Abb., 17 Tab., 23 Fotos	20,35
4	338	Meteorologie	LANZINGER, A. et al:	*Alpex-Atlas.* FWF-Projekt P6302 GEO, Wien 1991, 234 S., 23 Abb., 2 Tab., 200 Karten	18,17
5	341	Meteorologie	BÖHM, R.:	*Lufttemperaturschwankungen in Österreich seit 1775.* Wien 1992, 95 S., 34 Abb., 24 Tab.	vergriffen
6	343	Geophysik	MEURERS, B.:	*Untersuchungen zur Bestimmung und Analyse des Schwerefeldes im Hochgebirge am Beispiel der Ostalpen.* Wien 1992, 146 S., 72 Abb., 9 Tab.	11,63
7	351	Meteorologie	AUER, I.:	*Niederschlagsschwankungen in Österreich seit Beginn der instrumentellen Beobachtungen durch die Zentralanstalt für Meteorologie und Geodynamik.* Wien 1993, 73 S., 18 Abb., 5 Tab., 6 Farbkarten	23,98
8	353	Meteorologie	STOHL, A., H. KROMP-KOLB:	*Analyse der Ozonsituation im Großraum Wien.* Wien 1994, 135 Seiten, 73 Abb., 8 Tabellen	23,98
9	356	Geophysik		*Tagungsbericht über das 6. Internationale Alpengravimetrie-Kolloquium, Leoben 1993.* Herausgeber: P. STEINHAUSER und G. WALACH, Wien 1993, 251 Seiten, 146 Abb.	23,98
10	357	Meteorologie	ZWATZ-MEISE, V.:	*Contributions to Satellite and Radar Meteorology in Central Europe.* Wien 1994, 169 Seiten, 25 Farbabb., 42 SW-Abb., 13 Tab.	23,98
11	359	Geophysik	LENHARDT W. A.:	*Induzierte Seismizität unter besonderer Berücksichtigung des tiefen Bergbaus.* Wien 1995, 91 S., 53 Abb.	23,98
12	361	Meteorologie	AUER, I., R. BÖHM, N. HAMMER †, W. SCHÖNER., WIESINGER W., WINIWARTER W.:	*Glaziologische Untersuchungen im Sonnblickgebiet: Forschungs-programm Wurtenkees.* Wien 1995, 143 S., 59 SW-Abb., 13 Farbabb., 9 SW-Fotos, 47 Tab.	23,98
13	372	Meteorologie	PIRINGER, M.:	*Results of the Sodar Intercomparison Experiment at Dürnrohr, Austria.* Wien 1996	23,98
14	373	Geophysik	MEURERS, B.:	*Proceedings of the 7th International Meeting on Alpine Gravimetry, Vienna 1996.* Wien 1996	23,98
15	374	Meteorologie	RUBEL, F.:	*PIDCAP - Quick Look Precipitation Atlas.* Wien 1996	23,98
16	378	Meteorologie	DOBESCH, H., KURY G.:	*Wind Atlas for the Central European Countries Austria, Croatia, Czech Republic, Hungary, Slovak Republic and Slovenia,* Wien 1997	23,98

Heft	Publ.Nr.	Fachgebiet	Autor	Titel und Umfang	Preis in Euro
17	382	Meteorologie		*Proceedings of the 9th International Symposium on Acoustic Remote Sensing and Associated Techniques of the Atmosphere and Oceans, Vienna 1998*, 329 Seiten, Wien 1998	23,98
18	383	Meteorologie	RUBEL, F.:	*PIDCAP - Ground Truth Precipitation Atlas.* 84 Seiten, 99 Farbkarten, Wien 1998	36,34
19	384	Meteorologie		*Proceedings of the 2nd European Conference on Applied Climatologie, 19 to 23 Oct. 1998, Vienna.* CD-ROM, Wien 1998	23,98
20	387	Meteorologie		*Proceedings of the 2nd International Conference on Experiences with Automatic Weather Stations, 27 to 29 Sept. 1999, Vienna.* CD-ROM, Wien 1999	23,98
21	388	Meteorologie		*Bericht über den Workshop Umweltforschung im Hochgebirge - Ergebnisse von GAW-Dach und verwandten Projekten, 05. bis 06. Okt. 1999, Wien.* 147 Seiten, Wien 1999	23,98
22	389	Meteorologie	DOBESCH, H., H. V. TRAN:	*The Diagnostic Wind Field Model ZAWIMOD2.* 47 Seiten, 8 Farbabb., Wien 1999	23,98
23	392	Meteorologie		*Proceedings of the 26th International Conference on Alpine Meteorology; 11 to 15 Sept. 2000, Innsbruck.* CD-ROM, Wien 2000	23,98
24	395	Meteorologie	SABO, P.:	*Hochnebelprognose mittels eines objektiven Inversionsindexes für die synoptische Praxis,* 80 Seiten, Wien 2000	23,98
25	397	Meteorologie	AUER, I., R. BÖHM, W. SCHÖNER:	*Austrian long-term climate 1767-2000 - Multiple instrumental climate time series from central Europe,* 160 Seiten, 31 Farbseiten, CD-ROM, Wien 2001	25,00
26	398	Geophysik	MEURERS, B.:	*Proceedings of the 8th International Meeting on Alpine Gravimetry, Leoben 2000,* 240 Seiten, 4 Farbseiten, Wien 2001	25,00
27	399	Meteorologie		*Proceedings of the Deutsch-Österreichisch-Schweizerische Meteorologentagung; 18 to 21 Sept. 2001, Vienna.* CD-ROM, Wien 2001	25,00
28	408	Meteorologie	AUER, I., R. BÖHM, M. LEYMÜLLER, W. SCHÖNER:	*Das Klima des Sonnblicks – Klimaatlas und Klimatographie der GAW Station Sonnblick einschliesslich der umgebenden Gebirgsregion,* 305 Seiten, 130 Farbabbildungen, CD-ROM, Wien 2002	50,00
29	409	Meteorologie		*Scientific Contributions of Austria to the Mesoscale Alpine Programme (MAP),* 74 Seiten, 38 Farbseiten, Wien 2003	25,00
30	411	Meteorologie	HUBER-POCK, F.:	*Die atmosphärischen Gleichungen in den meteorologischen Koordinatensystemen,* 160 Seiten, 1 Farbseite, Wien 2003	25,00
31	412	Geophysik	MEURERS, B., R. PAIL:	*Proceedings of the 1st Workshop on International Gravity Field Research, Graz 2003,* 204 Seiten, 3 Farbseiten, Wien 2004	25,00
32	413	Meteorologie	BAUMANN-STANZER, K.:	*Qualitätsprüfung, Verifikation und Anwendung von Windprofilerdaten in Österreich,* 133 Seiten, 29 Farbseiten, Wien 2004	25,00
33	414	Meteorologie	SPAN, N., A. FISCHER, M. KUHN, M. MASSIMO, M. BUTSCHEK:	*Radarmessungen der Eisdicke östereichischer Gletscher, Band I: Messungen 1995 bis 1998,* 154 Seiten, Wien 2005	25,00
34	415	Meteorologie	DOBESCH, H., D. NIKOLOV, L. MAKKONEN:	*Physical Processes, Modelling and Measuring of Icing Effects in Europe,* 75 Seiten, 18 Farbseiten, Wien 2005	25,00